10 Aug 2023

Crystal Environment Induced Symmetry Reduction (CEISR): Deep Analysis Of Para-chloroacetophenone Azine And Generalization

Harmeet Bhoday

Kaidi Yang

Steven P. Kelley

Rainer Glaser
Missouri University of Science and Technology, glaserr@mst.edu

Recommended Citation

H. Bhoday et al., "Crystal Environment Induced Symmetry Reduction (CEISR): Deep Analysis Of Para-chloroacetophenone Azine And Generalization," *CrystEngComm*, vol. 25, no. 33, pp. 4638 - 4657, Royal Society of Chemistry, Aug 2023.
The definitive version is available at https://doi.org/10.1039/d3ce00676j

Volume 25
Number 33
7 September 2023
Pages 4613–4770

CrystEngComm

rsc.li/crystengcomm

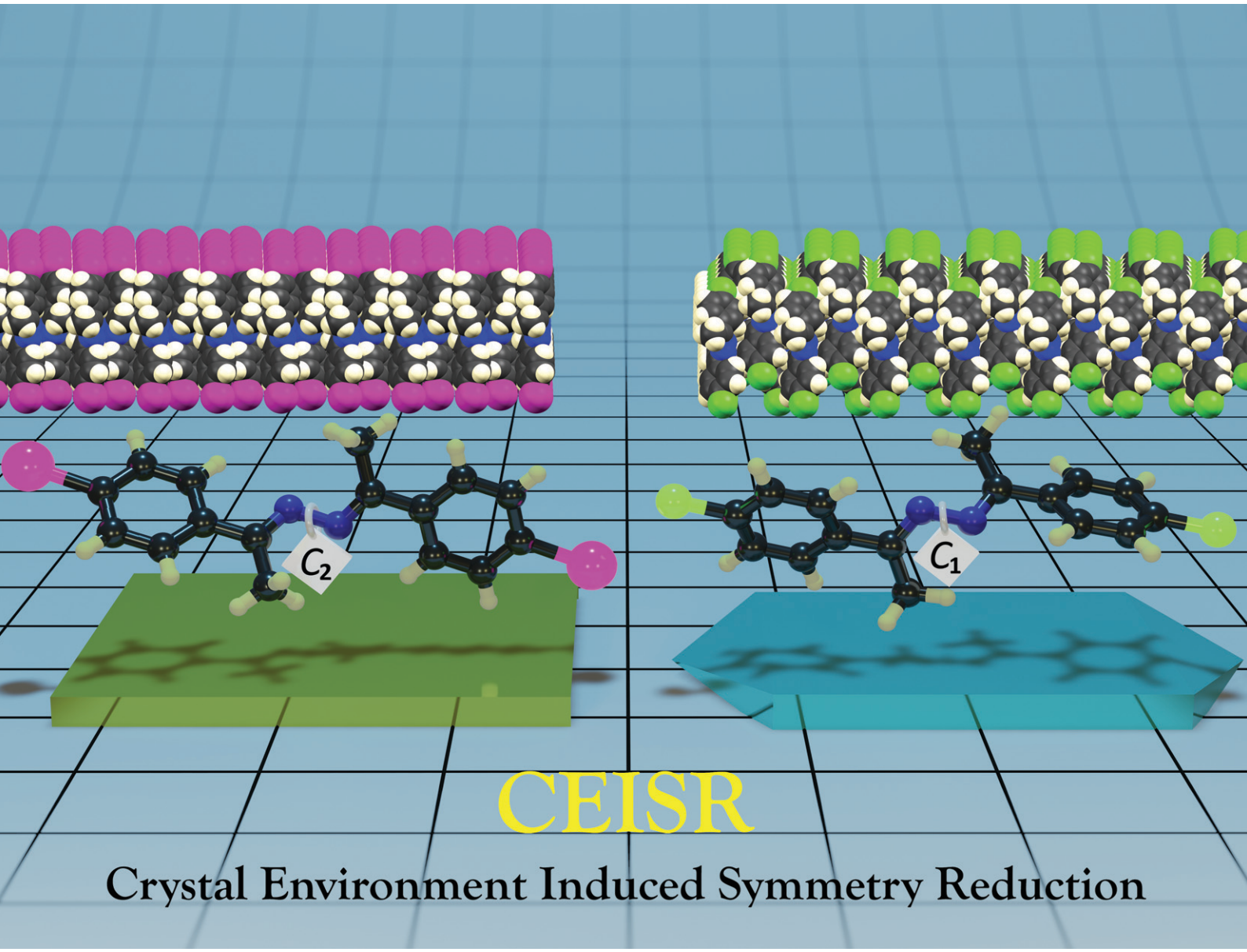

ISSN 1466-8033

ROYAL SOCIETY OF CHEMISTRY

PAPER

Rainer Glaser *et al.*

Crystal environment induced symmetry reduction (CEISR): deep analysis of *para*-chloroacetophenone azine and generalization

CrystEngComm

ROYAL SOCIETY OF CHEMISTRY

PAPER

View Article Online
View Journal | View Issue

Cite this: *CrystEngComm*, 2023, **25**, 4638

Crystal environment induced symmetry reduction (CEISR): deep analysis of *para*-chloroacetophenone azine and generalization†

Harmeet Bhoday, [a] Kaidi Yang, [ab] Steven P. Kelley [b] and Rainer Glaser *[a]

The morphologies of sixteen crystal structures of ten symmetrical X_{para}–Ph–(Me)C═N–N═C (Me)–Ph–X_{para} azines: **1** (Cl), **2** (Br), **3** (I), **4** (OH), **5** (PhO), **6** (CF_3), **7** (F), **8** (Me), **9** (NO_2), and **10** (PrO) are described. All the azines crystallize forming idioteloamphiphile monolayers (IAMs) and their morphologies fall into the two main classes of "flat" and "shiplap" depending on the lateral offsets between next-neighbors in the monolayer. *Ab initio* studies show that the (*E*,*E*)-configured *p*-disubstituted acetophenone azines are C_2-symmetric in the gas phase and that the azine and phenyl twists are correlated and give rise to *P*- and *M*-chirality. The crystal structures of **1**–**10** are true racemates and, remarkably, the majority feature asymmetric (C_1) azines rather than dissymmetric (C_2) azines. To understand the origin of the symmetry reduction, we studied the supramolecular structures and IAM characteristics of the five azines that crystallize with a flat morphology **1-I** (Cl), **2-Ia** (Br), **3** (I), **5** (PhO), and **10** (PrO). The deep analysis of chloroazine **1-I** shows that the symmetry reduction is the result of qualitatively different coordination environments of the two chloroarene moieties and presents a case of crystal environment induced symmetry reduction (CEISR). The crystal structure of **1-I** is of the type "AABB Kick/Flat" and the advantages of the double-stripe motif are explained. Careful analysis of the crystal structure showed arene–arene T-contacts of the types edge-to-face (e|f), face-to-edge (f|e), and face-to-face (f|f), a new arene–azine interaction (e|Az), and H···Cl, Cl···π, and Cl···Cl contacts. Intra- and interlayer interaction inventory analyses show in a compelling fashion that the arenes A_i and A_s in each azine engage in qualitatively different intermolecular interactions. To demonstrate the usefulness of the interaction inventory analysis, we also compare and contrast the crystal environments of the C_1-symmetric azines in crystals of **2-Ia** (Br) and **10** (PrO) and the C_2-symmetric azines in crystals of **3** (I) and **5** (PhO). Intermolecular interactions are quantified using Hirshfeld surface analyses, pairwise interaction energies, and electrostatic potential maps. We will also describe a fast method for the detection of CEISR based on N···H Hirshfeld 2D fingerprint plots.

Received 6th July 2023,
Accepted 27th July 2023

DOI: 10.1039/d3ce00676j

rsc.li/crystengcomm

1. Introduction

Azines belong to the group of organic compounds with the connectivity RR′C═N–N═CRR′, where R and R′ can be alkyl or aryl groups.[1] They are basically 2,3-diaza derivatives of butadienes and can also be considered as N–N connected diimines. Azines play important roles in crisscross cycloaddition[2] and heterocycle synthesis.[3] Extensive applications of azines have emerged in medicinal chemistry as neuroinflammatory agents,[4] antifungal agents,[5] anticancer agents,[6] and MDR reversal agents.[7] Azines are important precursors for the fabrication of conducting polymers to serve as cathode materials for organic batteries,[8] covalent organic frameworks for hydrogen evolution,[9] NLO-active photovoltaic materials,[10] organic field-effect transistors (OFET),[11] film transistors, *etc.*[12]

We have been interested in unsymmetrical donor–acceptor substituted azines D–Ph–(R)C═N–N═C(R)–Ph–A (Scheme 1, left) because of their non-linear optical properties. These materials stand out because we have been able to fabricate crystals with perfect dipole alignment in several acetophenone azine series RO–Ph–(Me)C═N–N═C(Me)–Ph–X_{para}. Initial success came with the methoxy series (RO = H_3CO) with X = Cl,[13] Br,[14] and I,[15] and we have since realized several materials in the phenoxy series (RO = PhO)[16–21] and

[a] *Department of Chemistry, Missouri University of Science and Technology, Rolla, Missouri, 65409, USA. E-mail: glaserr@mst.edu*
[b] *Department of Chemistry, University of Missouri, Columbia, Missouri, 65211, USA*

† Electronic supplementary information (ESI) available. CCDC 2027206, 2234130, 2241667 and 2251374. For ESI and crystallographic data in CIF or other electronic format see DOI: https://doi.org/10.1039/d3ce00676j

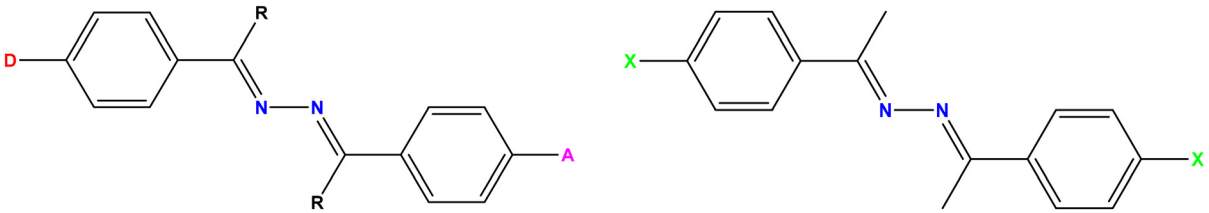

Scheme 1 1,4-Diphenyl azines are commonly derived from benzophenone (R = H) and acetophenone (R = CH_3). It is our goal to fabricate ferroelectric crystals of unsymmetrical azines with *para*-phenyl substitution by donors and acceptors. In the present paper, we focus on symmetrical azines with X = Cl, Br, I, PhO, and PrO.

the decyloxy series (RO = DecO).[22–25] The concepts guiding the fabrication of these ferroelectric materials have been described.[26–28] While our primary interest has always been with unsymmetrical azines, we have also studied intensively symmetrical azines to learn about the intermolecular interactions in azine crystals.[29–36]

Here we report on the supramolecular structure of a series of symmetrical azines (Table 1). First, we will discuss the morphologies of idioteloamphiphile monolayer architectures (IAMs) of azines and show that they fall into two major classes described as flat and shiplap. Second, we report on the supramolecular structure of polymorph **I** of *para*-chloroacetophenone azine **1** (Scheme 1, right). We reported polymorph **1-Ia** many years ago[30,37] and the recent crystallization of polymorph **1-II** (ref. 38) called for a careful comparison of the polymorphism. Third and most importantly, the deep analysis of flat **1-I** reveals an unexpected feature of the crystal packing. We will show that **1** adopts a C_2 symmetric structure (dissymmetric) in the gas phase. A cursory analysis also might suggest the occurrence of dissymmetric azine molecules in the crystal structure. However, careful analysis reveals that the azine molecules experience an asymmetric environment causing the inequivalence of their two arenes. This inequivalence was initially revealed because of the recognition that only one arene of every azine engages in an arene–azine contact. To make this point in a comprehensive fashion, we will describe the full intralayer and interlayer interaction inventories of the two arenes in one azine molecule. The next-neighbor analysis demonstrates in a compelling fashion that the two arenes serve entirely different purposes in the layer architecture of the crystal. A survey of sixteen crystal structures of ten symmetrical azines shows that C_2 symmetry is the exception and crystal environment induced symmetry reduction (CEISR) occurs in twelve of those cases (Table 1).

The results of interaction inventory analyses are also provided for other flat azines **2-Ia** (Br),[39] **3** (I),[40] **5** (PhO),[41] and **10** (PrO)[42] to examine generality. The structural analyses focus on the topology of contacts between synthons, and the intermolecular interactions are quantified using Hirshfeld surface analyses, pairwise interaction energies, and electrostatic potential maps. We will also describe a fast method for the detection of CEISR based on N···H Hirshfeld 2D fingerprint plots.

2. Results and discussion

2.1. Correlations of azine and phenyl conformations

Azine **1**, 1,4-bis(*p*-chlorophenyl)-1,4-dimethyl-2,3-diazabutadiene, crystallizes with a monoclinic unit cell in the space group $P2_1/c$ and contains one independent molecule, see Fig. 1. The crystal structure of **1-I** was determined at 295 K (**1-Ia**) and 100 K (**1-Ib**)

Table 1 Overview of IAM types of symmetrical azines

#	X	CCDC code	CCDC #s	Temp.	IAM Type	Azine twist	Ph1 twist	Ph2 twist	Symm.	CEISR	Ref.
1-Ia	Cl	LIKHUI	1207287	295 K	AABB kick/flat	134.71	−29.31	−30.53	C_1	YES	*JOC*, 1994 [ref. 30]
1-Ib	Cl	LIKHUI02	2251374	100 K	AABB kick/flat	134.77	−28.96	−31.70	C_1	YES	This work
1-II	Cl	LIKHUI01	2027206	100 K	Ideal-shiplap/flat	180.00	−26.37	26.37	C_i	NO	This work
2-Ia	Br	LIKJEU	1207288	295 K	AABB kick/flat	131.85	−20.96	−27.26	C_1	YES	*JOC*, 1994 [ref. 30]
2-Ib	Br	LIKJEU03	2241667	100 K	AABB kick/flat	132.07	−29.39	−29.85	C_1	YES	This work
2-II	Br	LIKJEU02	2234130	150 K	Ideal-shiplap/flat	180.00	−26.33	26.33	C_i	NO	This work
3	I	LIZNEN	139916	173 K	Flat/flat-zigzag	141.82	−8.07	−8.07	C_2	NO	*JCC*, 1999 [ref. 33]
4	OH[a]	BITTIH	1111781	295 K	Shiplap/ideal-flat	148.37	19.57	12.82	C_1	YES	*JCS PT2*, 1995 [ref. 51]
5	OPh	KIGBAG	1838227	293 K	Ideal-flat	143.34	−12.47	−12.47	C_2	NO	*CSD*, 2018 [ref. 41]
6	CF_3	WEWMET	1843926	173 K	Shiplap/double flat	114.38	−2.34	10.42	C_1	YES	*CSD*, 2018 [ref. 35]
7	F	LIKHOC	1207286	295 K	ABB/shiplap	137.99	1.87	−18.61	C_1	YES	*JOC*, 1994 [ref. 30]
8	Me	PIYYAX	1235041	295 K	ABB/shiplap	142.76	0.45	−19.89	C_1	YES	*ACIEE*, 1994 [ref. 32]
9-Ia	NO_2	ZEHJUR	1310588	295 K	AABB shiplap/flat	152.00	1.21	13.98	C_1	YES	*JCS PT2*, 1995 [ref. 50]
9-Ib	NO_2	ZEHJUR02	984384	130 K	AABB shiplap/flat	155.22	−0.93	12.34	C_1	YES	*JCS*, 2015 [ref. 34]
9-II	NO_2	ZEHJUR01	984383	140 K	Shiplap/flat	113.37	2.0	11.78	C_1	YES	*JCS*, 2015 [ref. 34]
10	OPr	HUXMIZ	2027208	100 K	Flat	134.40	−6.85	−15.11	C_1	YES	*CSD*, 2020 [ref. 36]

[a] Crystallized as hydrate.

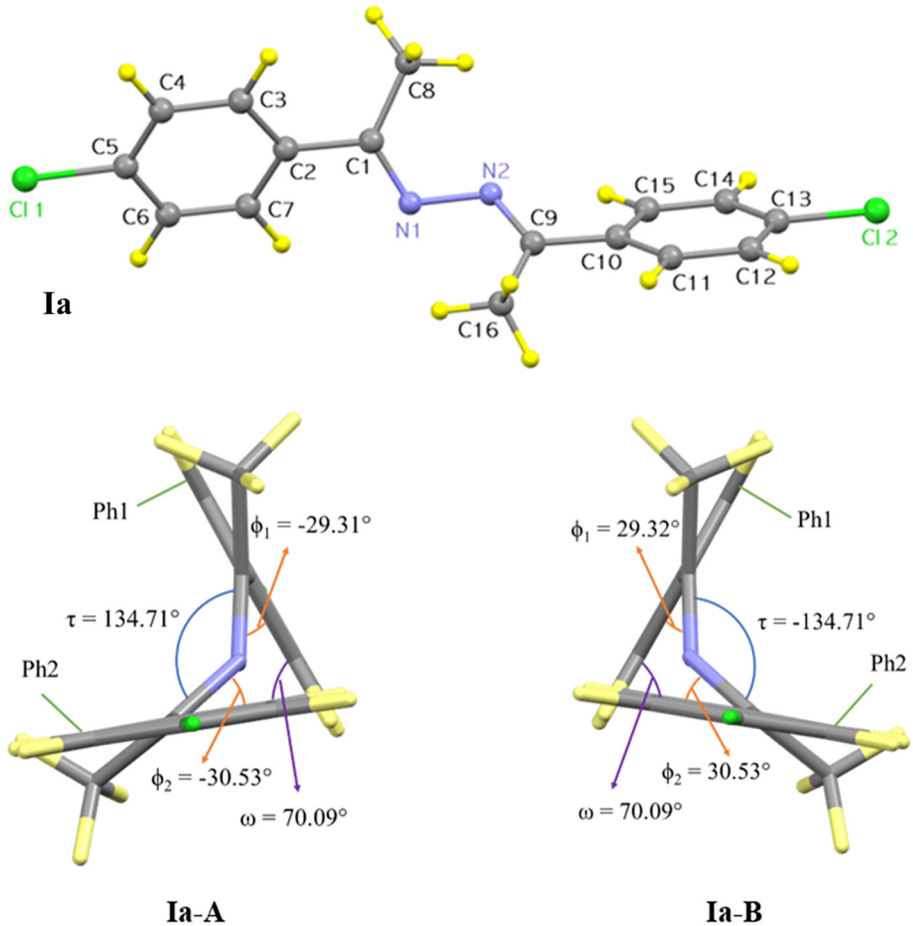

Fig. 1 ORTEP images of (*E*,*E*)-configured **1** azine in polymorphic form **I**. Newman projections viewed along the N–N bonds show the different helicities in enantiomers **I-A** (*P*-helicity) and **I-B** (*M*-helicity).

and we will discuss **1-Ia** or **I** for short. Form **I** contains two enantiomers **I-A** and **I-B** in equal numbers, that is, the crystal is a true racemate.[43] The azine is characterized by the torsion angle τ = ∠(C═N–N═C) and the phenyl twists ϕ_i, that is, the dihedral angles ϕ_1 = ∠(C7–C2–C1═N1) and ϕ_2 = ∠(C15–C10–C9═N2). In form **I**, the phenyl twists are conrotatory because the dihedral angles ϕ_1 = 29.32° and ϕ_2 = 30.53° have the same sign. Note the small difference in the twist angles.

The helicities of the C═N–N═C conformation (azine twist), the N1═C1–C2–C7 conformation (Ph1 twist) and the N2═C9–C10–C15 conformation (Ph2 twist) are defined as follows. For the C═N–N═C conformation, the helicity is referred to as *P* if a clockwise rotation is required about the N–N bond for the proximate C═N bond to eclipse the distal C═N bond and it is *M* if a counter-clockwise rotation is required.[44] For the phenyl twists at the two ends, *P*-helicity indicates that a clockwise rotation is required to eclipse the phenyl ring to the C═N bond while *M*-helicity indicates a counter-clockwise rotation. The helicities and the conformations of both **I-A** and **I-B** are shown in Table 2. Enantiomers **I-A** and **I-B** have *P*- and *M*-helicity about the N–N bond as shown in Fig. 1. The azine *P*-helicity of **I-A** occurs with phenyl twist *M*-helicities for Ph1 and Ph2.

In **I**, the helicities of the two Ph twists are always the same in each azine molecule, so the accumulation of τ, ϕ_1 and ϕ_2 causes the two phenyl groups to be in two planes that intersect with angle ω = 70.09° (Fig. 1).

Conformational preferences of the free azine **1** were studied with density functional theory (DFT)[45] at the APFD/6-311G* theoretical level, that is, we employed the Austin–Frisch–Petersson functional with dispersion (APFD)[46]

Table 2 Azine and phenyl twists in polymorph **I** of **1** and helicity[a,b]

	Molecule	I-A	I-B
Azine twist	Helicity	*P*	*M*
	Angle (τ)	+134.71	−134.71
	Conformation	+ac	−ac
Ph1 twist	Helicity	*M*	*P*
	Angle (ϕ_1)	−29.31	+29.32
	Conformation	−sp	+sp
Ph2 twist	Helicity	*M*	*P*
	Angle (ϕ_2)	−30.53	+30.53
	Conformation	−sc	+sc

[a] Conformation is described as anticlinal (ac), anticlinal (ac), antiperiplanar (ap), synperiplanar (sp), and synclinal (sp) based on the torsion angle of τ and ϕ. [b] See text for definition of twist angles.

together with the 6-311G* basis set.[47–49] Computations were performed with Gaussian 16 (ref. 50) on the high-performance computer system at the University of Missouri.

In the crystal structure of **I**, the helicity of the Ph twist is always opposite to the helicity of the azine twist. We wanted to know whether this feature is due to packing or whether we could locate additional minima with all possible permutations of azine and Ph helicities. Therefore, we performed APFD/6-311G* optimizations of **1** starting with the geometries of **I-A** and **I-B** but with opposite helicity of the Ph1 twist only ($\phi'_1 = -\phi_1$, $\phi'_2 = \phi_2$), with opposite helicity of the Ph2 twist only ($\phi'_1 = \phi_1$, $\phi'_2 = -\phi_2$), and with opposite helicity at both Ph1 and Ph2 ($\phi'_1 = -\phi_1$, $\phi'_2 = -\phi_2$). Information about the initial trial structures is provided in Table S1.† It was found that no matter what initial helicities were chosen, all optimizations returned to the C_2-symmetric enantiomers of **1**. We conclude that the Ph and azine twists are strongly correlated and exhibit the same correlation in the gas phase and the crystal structure.

2.2. Idioteloamphiphile monolayer architectures

We have previously discussed possible arrangements of idioteloamphiphile monolayers (IAMs) and of

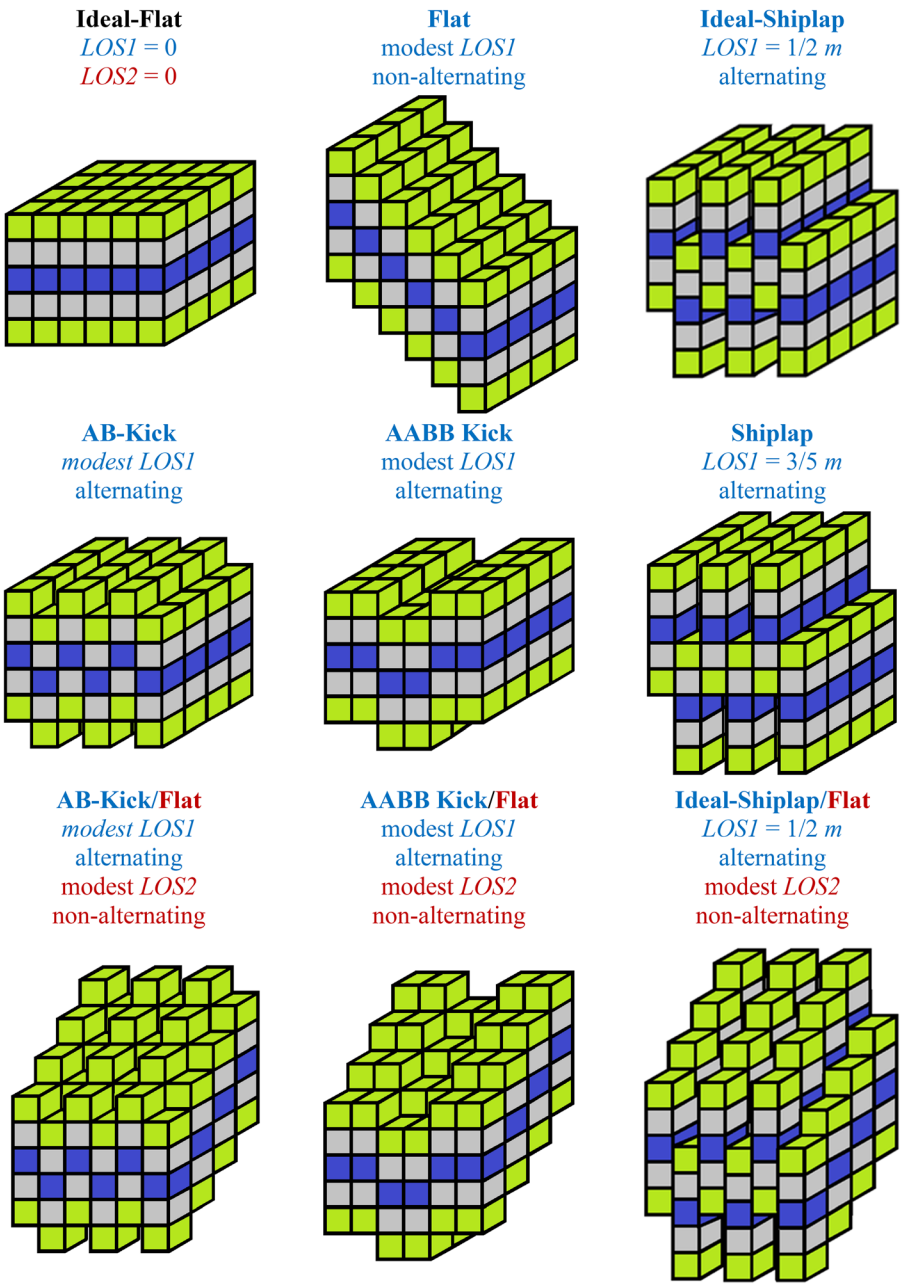

Scheme 2 Types of longitudinal offsets in IAMs.

beloamphiphile monolayers (BAMs).[19,23] Scheme 2 shows several options for IAMs. One symmetrical azine molecule is schematically represented by five units to indicate the substituents chlorine (green), the arenes (grey), and the azine bridge (blue). The simplest arrangement is the "ideal-flat" IAM, that is, all molecules are packed in the layer without any longitudinal offset *LOS* in either layer direction. The molecules are perpendicular to the layer surfaces and the

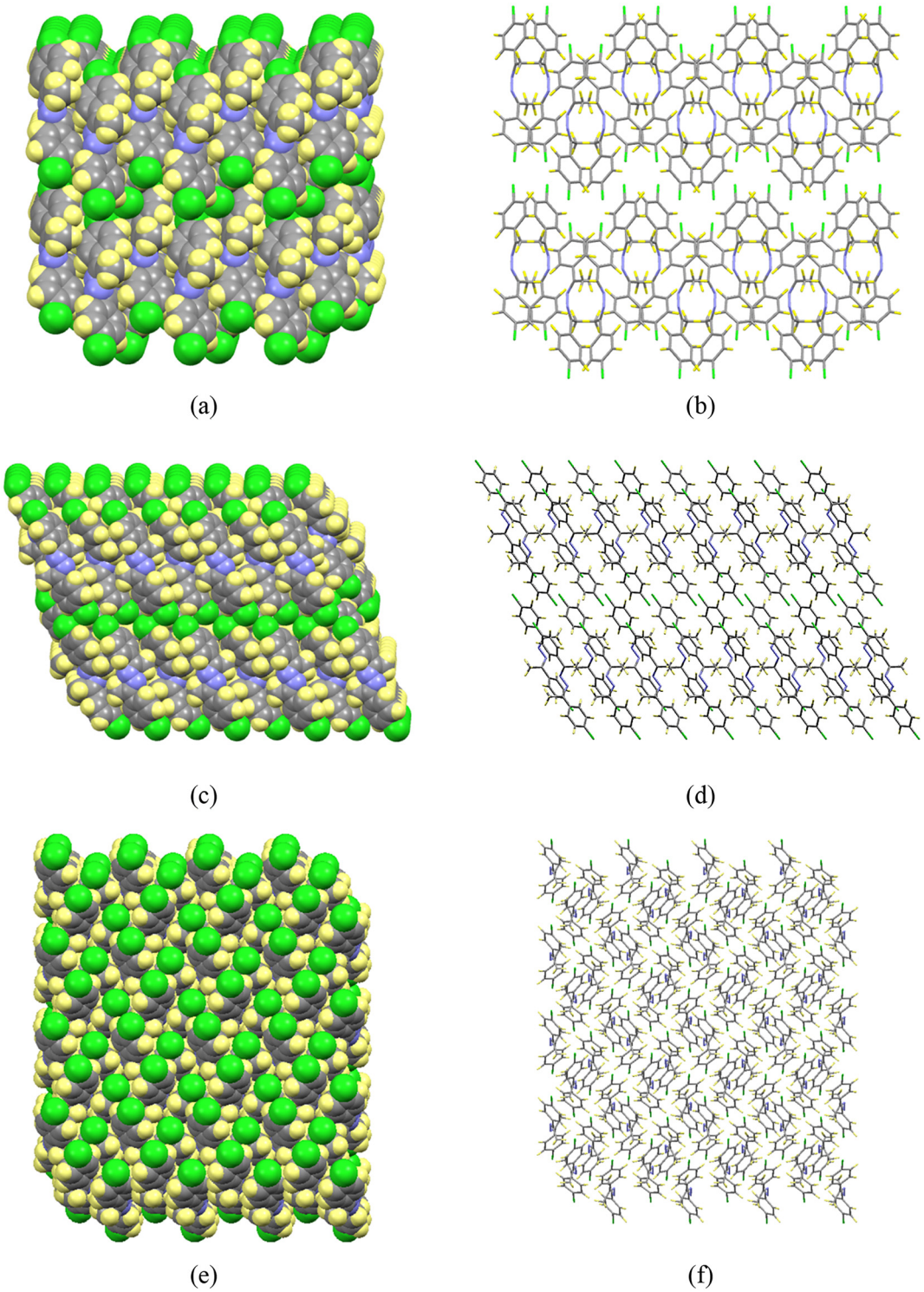

Fig. 2 Crystal alignment of **1** polymorph **I** in four layers. Space filling models (left) and tube models (right) are shown. (a and b) View down the *c* axis with the *b* axis pointing to the right and the *a* axis pointing up (top row). (c and d) View down the *b* axis with the *a* axis pointing up and the *c* axis pointing to the left (middle row). (e and f) View down the *a* axis with the *c* axis pointing down and the *b* axis pointing to the right (bottom row).

molecule length m equals the distance between the IAM surfaces. We refer to a stripe as a slice of an IAM along either one of the IAM directions.

The longitudinal offset of a neighboring molecule is relative to the long axis of the parent molecule. We define an "non-alternating" offset if the offset direction is the same from one molecule to the next in the same layer direction. And "an alternating" offset occurs if the offset direction alternates from one molecule to the next in the same layer direction. The "flat" motif exemplifies a non-alternating offset in one layer direction (*LOS1*). Equivalently, the flat motif may be viewed as resulting from slanting all molecules relative to the IAM surface in one layer direction.

The "shiplap" motif exemplifies an alternating offset in one layer direction (*LOS1*) and Scheme 2 shows a general "shiplap" motif with a large *LOS1* = 3/5 m offset and the special case of the "ideal-shiplap" motif where *LOS1* = 1/2 m. The "ideal-shiplap" motif is realized in some other symmetrical azines[51] including **1-II** and **2-II**.[52] Arrangements with shiplap motifs with large *LOS* values can hardly be described as traditional monolayers. However, shiplap-like arrangements with small offsets do form monolayers. The "AB-Kick" and "AABB-Kick" motifs are special shiplap-type IAMs with small *LOS1* values. The AABB-Kick architecture essentially is a double-stripe shiplap motif. The variation "AABB-Kick/Flat" combines the AABB-Kick motif in one layer direction (modest *LOS1*) with flat stripes (modest *LOS2*) in the orthogonal layer direction (Scheme 2, bottom center) and this layer architecture is central to the understanding of polymorph **I**.

The description of Scheme 2 provides a rough overview of layer morphologies. In the following sections, we will add details about intralayer interactions, that is, the lateral interactions within the stripes in both layer directions and discuss the stacking of the IAMs and interlayer interactions.

2.3. Crystal packing of polymorph I

The IAM of polymorph **I** is of the AABB-Kick/Flat type and the layer directions are aligned with the crystallographic b and c axes and the layers are stacked in the a direction. The AABB-Kick motif in the b direction is shown beautifully by the space-filling model in Fig. 2a, and the flat nature of the stripes in the c direction results in the slanting seen in Fig. 2c.

The near C_2-symmetry of the unique molecule in polymorph **I** might lead one to assume that the two arenes in each azine molecule are more or less equivalent. In particular, one might expect that the intermolecular interactions of each arene with its neighborhood are essentially the same. Attentive readers may have noticed that the phenyl twists ϕ_1 = 29.32° and ϕ_2 = 30.53° are slightly but significantly different in polymorph **I** (Fig. 1). In fact, we will demonstrate that the intralayer coordination modes of the two arenes in one azine molecule differ greatly. This will be accomplished by analysis of the intralayer pairs **Q**–**W** as well as the interlayer pairs **X** and **Y**. The entire analysis is made from the perspective of one azine molecule denoted by *, which we chose to have *P* helicity, and the analysis results in the interaction inventory of Table 3.

2.3.1. Double-T contacts stabilize the double-stripes. We now refine the discussion of the packing of polymorph **I** with the help of Fig. 3. The double-stripes AA and BB are shown together with their respective single stripes. Every stripe contains azine molecules stacked along the c direction. Inspection of Fig. 3 shows that the "AA" and "BB" double-stripes each contain one stripe composed entirely of azine with *M* helicity and another one with *P* helicity. The double-stripe is energetically favorable because it allows for strong double-T contacts between the molecules in both stripes.

A T-contact between two arenes involves CH···π interaction and may involve one C–H bond pointing toward the center of an arene face (^{1}T). The geometry of the benzene

Table 3 Intralayer and interlayer interaction inventory of **1-I**

X	*(*P*)	Neighbors of the starred molecule[a]							
Cl		**Q**(*M*)	**T**(*M*)	**R**(*M*)	**U**(*M*)	**V**(*P*)	**W**(*P*)		
Intra IAM	A_i^*	f|e(A_s)	e|f(A_i)	Cl|Me(A_s)	f|e(A_s)	vdW[b]	e|Az		
	A_s^*	e|f(A_i)	f|e(A_s)	Me|Cl(A_i)	e|f(A_i)	vdW[b]	vdW[b]		
	Az*				Az|Me(A_i)	Az|e(A_i)			
					Me(A_i)|Az				
		$\mathbf{Z}_i'(M)$	$\mathbf{Z}_1(M)$	$\mathbf{X}(M)$		$\mathbf{Z}_2(P)$	$\mathbf{Z}_2(P)$	$\mathbf{Y}'(P)$	$\mathbf{Y}(P)$
Inter IAM	A_i^*	Cl|e(A_s)						Cl|Cl(A_s)	
	A_s^*		e|Cl(A_i)	f|Cl(A_s) & Cl|f(A_s)		e|Cl(A_s)	Cl|e(A_s)		Cl|Cl(A_i)

[a] See Fig. 5 for definition of intralayer neighbors **Q**–**W** and Fig. 6 for definition of interlayer neighbors **X**–$\mathbf{Z}_2$. [b] vdW = non-specific van der Waals interaction.

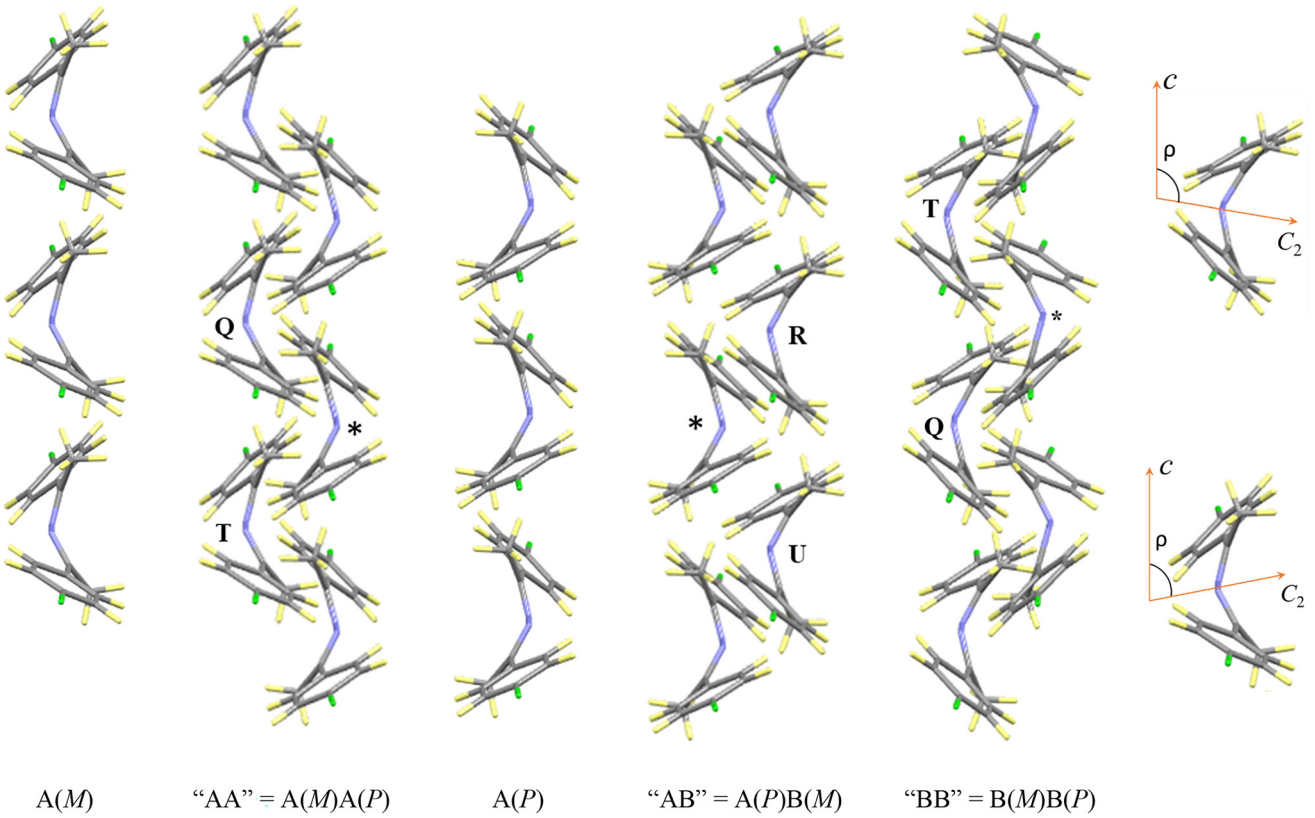

Fig. 3 The subtle difference between the AA and BB double-stripes is due to the different rotations of the azines about the *a* direction. See text for details.

dimer in the gas phase involves a ^{1}T-contact.[53] However, in the crystal structures of benzene a new type of T-contact occurs.[54] In this T-contact, the geometry of neighboring arenes involves an arene edge of the C–H donor to be almost parallel to an arene face and creates a ^{2}T-contact. Such a ^{2}T contact may involve one C–H bond or two C–H bonds of the arene edge (e) to engage in CH$\cdots\pi$ interactions with an arene face (f). For the characterization of such an edge-to-face T-contact (e|f), it suffices to specify the distance between the arene center and the closest C–H hydrogen. Unless otherwise noted, all ^{2}T-contacts discussed in the following are simply referred to as T-contacts and denoted as (f|e) or (e|f). This nomenclature is used in Table 3 where column 2 refers to the arene of the starred molecule in position 1 and the arene of the neighbor in position 2 is listed explicitly.

A double T-contact occurs if the arene moieties of one azine forms two T-contacts with a neighbor.[23] For a twisted azine, one arene functions as a face (f) in a T-contact while the other arene serves as an edge (e). The neighboring molecule uses one arene as a face and one as an edge, but in the opposite direction. The double T-contact comes in two varieties, the closed and the open forms. In the closed form, the arene edge that is close to the methyl group engages in the T-contact whereas in the open form, the arene edge that is close to the azine-N engages in the T-contact.

The difference between the AA and BB double-stripes is subtle. Note that none of the C_2 axes of the azines in double-stripe AA or BB are parallel to the *b* direction. Instead, in the AA double-stripe, the *M* molecules all are rotated a few degrees counterclockwise around the *a* direction whereas the *P* molecules are rotated in the opposite direction. As a consequence, the angle ρ enclosed between the *c* direction and any of the C_2 axes will be smaller than 90° for the AA double-stripe. In the BB double-stripe, all rotations about the *a* direction are opposite to what they are in the AA double-stripe with the result that $\rho > 90°$. The AB interface is illustrated by the A(*P*)B(*M*) double stripe (Fig. 3). We have already discussed each of the stripes, and the only novelty concerns the formation of an open double-T contact between the stripes.

The starred molecule in the double stripe AA is engaged in two next neighbor interactions with the molecules **Q** and **T** as well as the two next neighbor interactions **R** and **U** in the adjacent B stripe. Any molecule in any stripe interacts with four neighbors with the same four interactions. The BB stripe in Fig. 3 results from the rotation of the AA stripe around the *b* axis and illustrates the presence of the same **Q** and **T** pairs.

2.3.2. Arene–azine contacts and enantiopure directed chains. A second, and unexpected, intermolecular interaction in our crystals is the arene–azine contact shown in Scheme 3. An arene–azine contact occurs between the azine bridge (–C(Me)═N–N═C(Me)–) of one molecule and a phenyl ring of an adjacent molecule. We have reported an *ab initio* study of the quadrupole moment of the parent

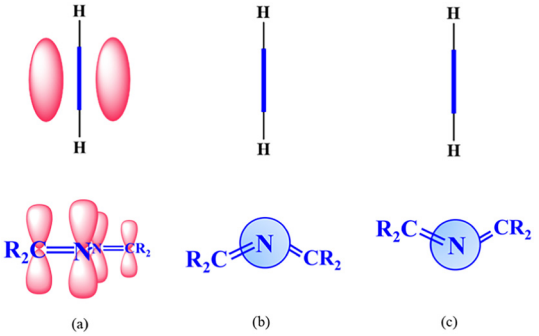

Scheme 3 An arene–azine contact e|Az involves the approximate edge-to-face alignment of one arene edge with the azine face with the arene edge approaching the N–N bond. (a) The e|Az contact with a planar azine. An azine with an azine twist may engage in either (b) a convex e|Az contact or (c) a concave e|Az contact.

azine, $H_2C{=}N{-}N{=}CH_2$, and we showed that the azine group is highly quadrupolar.[55] The illustration in Scheme 3a depicts an e|Az contact with a planar azine; the π clouds of the arene and the azine which are the negative pole regions surrounding the positive pole region containing the atoms are shown. In fact, on a per electron basis, the azine functional group is almost as quadrupolar as benzene. For a twisted azine, two options could be realized as shown in Scheme 3b and c.

In crystals of **I**, only the concave e|Az option is observed. Each azine molecule engages in two e|Az contacts serving as an azine receptor in the contact with neighbor **V** and as an arene edge in one contact with neighbor **W** (Fig. 4). The result of the e|Az contacts is a directed e|Az bonded chain of azines. Note that all three molecules in Fig. 4 are the same enantiomer (*P*) and that the molecule in the center is flipped around the direction of the e|Az bonded chain. In Fig. S1 (ESI†), we show two adjacent anti-parallel e|Az bonded chains.

2.3.3. Arene interaction inventory: inside and surface arenes. It is crucial to realize that it is only one arene of every azine that engages in such an e|Az contact and, moreover, it is the same arene in every molecule. It was this insight into the arene–azine contacts that shattered the assumption that the arenes in the near-C_2 azine experience the same environments. The coordination modes of the inside arene (A_i) and the surface arene (A_s) differ greatly, and it is only the inside arene A_i that engages in one e|Az contact while the surface arene does not. All next-neighbor interactions of A_i^* and A_s^* of the starred molecule are shown in Fig. 5, and their analysis allows for the completion of the intralayer interaction inventory of Table 3. Here and in similar tables below, arene–arene T-contacts are highlighted in red, interactions between an arene edge and an azine moiety are listed in blue, and contacts between arene and a substituent atom are listed in green. Special attention will be paid to the arene interaction inventories of A_i and A_s to demonstrate their inequality or equality.

In Fig. 5a, we show one slab of the IAM of polymorph **I** with five stripes and one molecule in stripe 3 is marked by

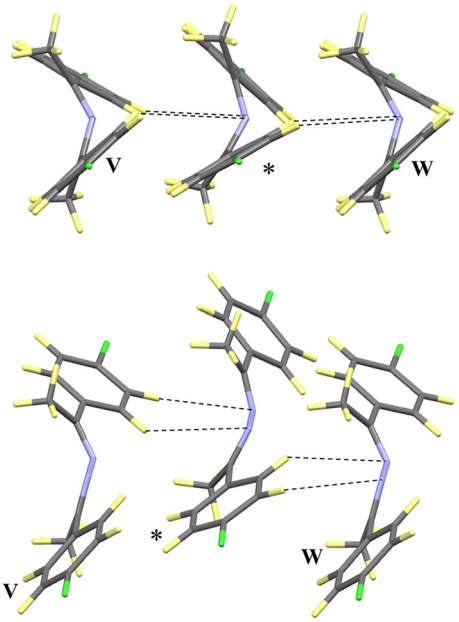

Fig. 4 Two perspectives of an aggregate of three azines are shown with dashed lines indicating short distances in two concave e|Az contacts. The starred molecule in the center engages its azine moiety in an e|Az contact with the distal arene on the left (**V**) and it also engages its proximate arene moiety with the azine moiety of its neighbor to the right (**W**).

"*" and surrounded by eight azines. The starred molecule and the two molecules marked **S** all belong to the same stripe, and the interaction of the starred molecule with either one of the molecules **S** must be the same. We refer to the pair interaction between the starred molecule and one of its neighbors by the label of that neighbor. Pair **S** is shown in Fig. 5b and it is a stacked dimer with flat offset *LOS2*. While the stripe motif is the preferred building block to describe the lattice architecture, the binding within the stripe is negligible with the centers of stacked arenes more than 10 Å away from each other. The molecules in stripe 3 are stabilized by their interactions with the proximate molecules in the directly attached stripes (stripes 2 and 4) and in the second-nearest stripes (stripes 1 and 5).

We began with an analysis of the coordination of the inside arene of the starred molecule A_i^*. Stripe 2 forms double-T contacts with stripe 3 and their ρ angles identify this double-stripe as a BB type. Molecules **Q** and **T** engage in modest offset double-T contacts with the starred molecule, see Fig. 5c. Arene A_i^* engages as a face in a T-contact with the edge of the A_s(**Q**); this $f(A_i)|e(A_s)$ contact is abbreviated as "f|e(A_s)" in Table 3. The same arene A_i^* engages as an edge in a T-contact with the face of the A_i(**T**); "e|f(A_i)" for short. Molecules **R** and **U** in stripe 4 are easily identified as belonging to an A stripe and the pairs **R** and **U** (Fig. 5d) are vastly different. The geometry of pair **R** may formally be described as a pair of methyl halogen contacts Cl|Me(A_s). The dimer **U** features a beautiful open double-T contact in which the face of A_i^* forms an f|e(A_s) contact. Note that all these

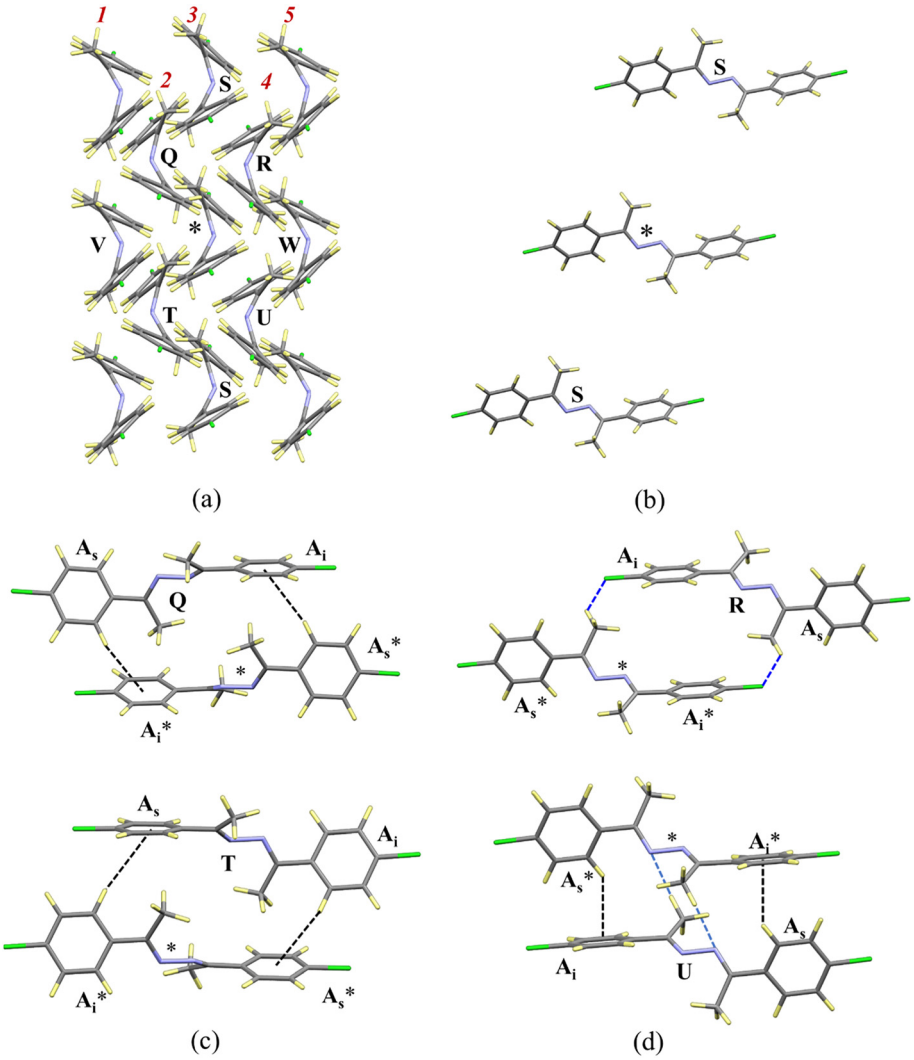

Fig. 5 The starred molecule **1** in polymorph **I** interacts with six neighbors using five types of interactions **Q**, **R**, **S**, **T** and **U**. (a) IAM structure viewed down the N–N bond axis (*a* axis). (b) Stripe 3 is shown along the *b* direction and illustrates **S** type pairing. (c) The pairing of the starred molecule in stripe 3 with molecules **Q** and **T** of stripe 2 is shown along the *b* direction. (d) The pairing of the starred molecule in stripe 3 with molecules **R** and **U** of stripe 4 is shown along the *b* direction.

intralayer edge contacts involve just one of the edge hydrogens, namely the hydrogen in the *ortho* position (H_o) with respect to the azine, and such edges are abbreviated as e_o. We will see later that the meta hydrogens (H_m) may be engaged in interlayer contacts with e_m edges. While the Me(A_s) methyl groups engage halogens in **R**, the Me(A_i) methyl groups engage azine-N in **U** and the Me(A_i)|Az and Az|Me(A_i) contacts are shown in Fig. 5d.

In Table 3, a border is drawn around pairs of T-contacts between the starred molecule and the same neighbor and they define a double T-contact. For example, the double T-contact of the starred molecule with neighbor **Q** includes the $f(A_i^*)|e(A_s)$ and $e(A_s^*)|f(A_i)$ T-contacts. Molecules **Q** and **T** engage in closed double T-contacts (shaded light red) while molecule **U** forms an open double T-contact (shaded light blue). The comparison of the rows for A_i^* and A_s^* shows that the inside arene A_i^* engages in two T-contacts as an edge (e|$f(A_i)$, e|Az) and in two more T-contacts as a face (both f|$e(A_s)$). The surface arene A_s^* also engages in two T-contacts as an edge (both e|$f(A_i)$), but only in one T-contact as a face (f|$e(A_s)$). Therefore, the arene interaction inventory reflects in a compelling fashion that the coordination modes of the two arenes of **1** are not equivalent. While it was the analysis of the arene–azine contacts that initially brought this inequivalence to the fore, the analysis of the arene–arene contacts is easier to perform and therefore advantageous to examine arene equivalence or inequivalence.

2.3.4. IAM stacking interaction. The remaining face of the surface arene A_s^* engages in face-on type Cl···π interlayer interaction with neighbor **X**, f|Cl(A_s) in Table 3. The f|Cl(A_s) contact is associated with a contact between the chlorine substituent $Cl(A_s^*)$ and the face of the A_s arene in neighbor **X**. At the same time, the arene A_s engages in the same type of contact with the chlorine of the same neighbor, Cl|f(A_s). In

addition, the Cl atom on A_s^* engages in interlayer halogen bonding with Cl(A_i) of neighbor **Y** (right in Fig. 6a). For the Cl atom of A_i^*, the interlayer halogen bonding interaction with Cl(A_s) of neighbor **Y′** is the only important contact (left in Fig. 6a).

Fig. 6b shows four interlayer contacts of the type Cl|e between a chlorine of one chloroarene and one hydrogen of the other chloroarene (the edge-H *meta* to the azine). Again, the A_s arene is much more engaged in these kinds of interlayer interactions compared to the A_i arene; A_s engages in three Cl|e contacts (right in Fig. 6b) while A_i engages in only one (left in Fig. 6b). The chloroarene with A_s serves as an e|Cl(A_i) contact with a $\mathbf{Z_1}$ neighbor and it serves both as Cl|e(A_s) and e|Cl(A_s) contacts with two $\mathbf{Z_2}$ neighbors. A_i^* engages only in one such contact Cl|e(A_s) with $\mathbf{Z_1'}$.

2.3.5. Quantifying structural parameters of intermolecular interactions. We want to supplement the topological analysis of intermolecular interactions with quantitative measures. In Table 4, all of the discussed pair interactions are characterized with a focus on chlorine–chlorine, arene–arene, and arene–chlorine distances: d(Cl*···Cl), d(Ph*···Ph), d(Cl*···Ph), and d(Ph*···Cl). We also characterize the shortest distance between the arene center and the proximate edge H atom (H_e): $d(H_e^*\cdots Ph)$ and d(Ph*···H_e). For contacts **V** and **W**, the distances are given between the center of the N–N bond and the closest proximate H_e atom: $d(H_e^*\cdots Az)$ and d(Az*···H_e). The most important distances are shown in the red face. For contacts $\mathbf{Z_1}$ and $\mathbf{Z_2}$, the distances are given between the chlorine atom and the proximate edge H atom (H_e): $d(H_e^*\cdots Cl)$ and d(Cl*···H_e).

The Cl···π interaction between the Cl–A_s moieties is of the face-on type.[56,57] The distance between the Cl atom of the starred molecule and the center of the arene of the **X** is d(Cl*, A_s[X]) = 3.86 Å, and the distance between the centers of the two arenes is $d(A_s^*, As[X])$ = 4.51 Å. The Cl atom of the Cl–A_s moiety of the starred azine also interacts with the Cl atom of the Cl–A_i moiety of interlayer neighbor **Y** (Fig. 6a). This Cl interaction is characterized by the very short non-bonded distance d(Cl···Cl) = 3.34 Å. The van der Waals radius of chlorine is 3.70 Å,[58] and the very short distance between the chlorines suggests rather strong halogen bonding.[59] Note that the comparable non-bonded Cl···Cl distance in the crystal of chlorobenzene is 3.7 Å.[60]

Our topological discussion was based on the analysis of arene–arene interactions and T-contacts in particular. While this approach is conceptually appealing, a more refined analysis requires the consideration of chloro–arene contacts. With the exception of the two long Cl···Cl distances of pairs **S** and **R**, all Cl···Cl distances are significantly shorter than their van der Waals distance of 7.4 Å.[51] We already stressed the rather short interlayer Cl···Cl contact of 3.34 Å in pair **Y**. Also, of note is the intralayer Cl···Cl contact of 4.73 Å in pair **U**.

Interlayer bonding is provided by C–H···Cl contacts[61,62] between *para*-Cl and *meta*-CH groups (Fig. 6b). The C–H···Cl contacts are reasonable if the distance d(Cl···H) is shorter than 3.35 Å. The Cl atom of the Cl–A_i moiety of the starred azine interacts with the H atom of interlayer neighbor $\mathbf{Z_1'}$ with the very short non-bonded distance d(Cl*···H) = 2.92 Å (red dots, Fig. 6b). A similar contact involves the A_s moiety of the starred molecule, where the arene A_s^* provides its hydrogen to form a contact with the Cl atom of neighbor $\mathbf{Z_1}$. Arene A_s^* forms two more C–H···Cl contacts with the neighbors $\mathbf{Z_2}$ and the distance d(Cl*···H) = d(H*···Cl) = 3.36 Å (green dots, Fig. 6b).

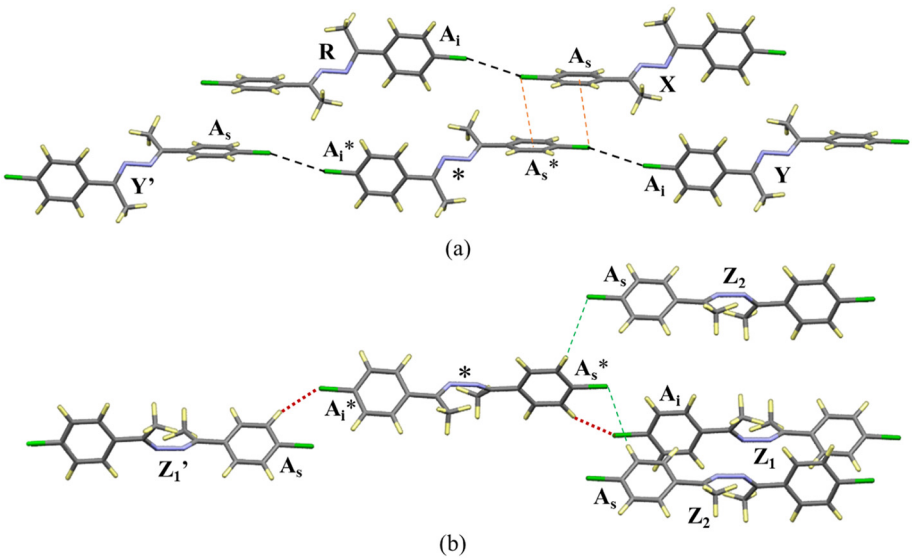

Fig. 6 In (a) the surface arene A_s^* engages in one face-to-face stacking interaction with the surface arene of the interlayer neighbor **X**. Halogen bonding contacts occur between the Cl atoms attached to A_s^* and A_i^* with the inside arene of neighbor **Y**, A_i[**Y**], and the surface arene of neighbor **Y′**, A_s[**Y′**], respectively. In (b) A_s^* engages in three H···Cl contacts but A_i^* only engages in one such contact.

Table 4 Intermolecular distances characterizing intra- and interlayer chloroarene pair interactions in polymorph I[a,b,c,d,e]

	Cl*···Cl	Ph*···Ph	Cl*···Ph	Ph*···Cl	$H_e^*\cdots\left(\frac{Ph}{Az}\right)$	$\left(\frac{Ph}{Az}\right)^*\cdots H_e$	$H_e^*\cdots$Cl	Cl*···H_e
$(A_i–Cl)^*$								
S	10.46	10.46	8.99	12.55	8.79	8.78	11.17	7.96
Q	5.86	5.71	4.90	7.89	5.68	3.77	7.18	3.44
T	5.86	5.71	7.89	4.90	3.77	5.56	3.44	7.18
R	8.44	8.51	6.12	11.20	6.74	7.57	9.59	5.39
U	4.73	**4.86**	5.19	6.19	5.15	4.40	5.72	3.04
V	6.05	5.99	4.74	8.33	3.13	**2.99**	3.46	3.46
W	6.22	6.28	4.77	8.65	**2.99**	3.13	3.37	3.37
Y′	**3.34**	9.46	6.38	6.38	NA	NA	5.44	5.40
$\mathbf{Z_1'}$	4.29	7.56	5.31	5.28	NA	NA	3.05	**2.92**
$(A_s–Cl)^*$								
S	10.46	10.46	12.55	8.99	9.20	9.18	7.96	11.17
Q	5.96	5.87	7.99	5.05	3.56	5.49	3.31	7.40
T	5.96	5.87	5.05	7.99	5.49	3.56	7.24	3.26
R	8.44	8.51	11.20	6.12	7.57	6.74	5.39	9.59
U	4.73	**4.86**	6.19	5.19	4.75	5.15	3.04	5.72
V	6.22	6.28	8.64	4.77	7.01	6.67	6.74	6.74
W	6.05	5.99	8.33	4.74	6.67	7.01	6.38	6.38
X	5.37	**4.51**	**3.86**	**3.86**	NA	NA	4.03	4.03
Y	**3.34**	9.46	6.38	6.38	NA	NA	5.40	5.44
$\mathbf{Z_1}$	4.29	7.56	5.28	5.31	NA	NA	**2.92**	3.05
$\mathbf{Z_2}$	4.83	7.24	5.22	5.22	NA	NA	3.36	3.36

[a] All distances are in Ångström. [b] Column "Cl*···Cl" lists the intermolecular Cl···Cl distances in a chloroarene pair. [c] Column "Ph*···Ph" lists the intermolecular distances between the centers of the arenes in a chloroarene pair. [d] Columns "Cl*···Ph" and "Ph*···Cl" list the intermolecular distances between the chlorine of one chloroarene and the center of the other. [e] Columns "H_e^*···Ph" and "Ph*···H_e" list the intermolecular distances between the center of one chloroarene and the closest edge H of the other. For **V** and **W**, the values "H_e^*···Az" and "Az*···H_e" specify the distance between an edge H and the center of the azine N–N bond.

The geometry of the benzene dimer in the gas phase was measured by microwave spectroscopy and the ^{1}T-contact is characterized by a distance between the arene centers of 4.96 Å.[46] For the crystal structure of benzene, the ^{2}T-contact features a C–H···π distance of 2.96 Å and an arene–arene distance of 5.05 Å.[47] For chlorobenzene, the ^{1}T-contact features a C–H···π distance of 2.81 Å and an arene–arene distance of 4.92 Å (CCDC number: 1050587).[53] In a ^{2}T-contact, the typical distance between the center of the face arene and the proximate edge-Hs is 2.91 ± 0.12 Å (ref. 63) and the typical distance between the arene centers is 4.85 ± 0.15 Å. Strong face-to-face contacts are characterized by arene–arene distances of typically 3.7 ± 0.3 Å.[64–66] *Para*-chloroacetophenone exemplifies a donor–acceptor substituted benzene and its crystals feature an arene stacking distance of 4.01 Å (CCDC number: 248149).[67]

We cast the topological analysis in terms of double T-contacts **Q**, **T**, **R**, and **U** as an explanatory device. Only numbers shown in Table 4 in red and bold face indicate strong arene–arene interactions. It becomes immediately clear that only the pair interaction **U** is a strong double T-contact, while pairs **Q** and **T** are marginal double T-contacts at best. Intralayer Cl···Cl interactions are unimportant and there is only strong interlayer Cl···Cl interaction associated with pair **Y**. Finally, the data in Table 4 demonstrate that the Cl···π interactions are only important for the interlayer interaction **X**.

2.4. CEISR concept and its generality

We have demonstrated the origin of the symmetry reduction of azine **1** from C_2 to C_1 and we have shown in a compelling fashion that the arenes A_i and A_s in each azine engage in qualitatively different intermolecular interactions. The packing related molecular symmetry reduction described for chloroazine **1** results from qualitatively different coordination environments of moieties that otherwise could be symmetric. We refer to this consequence of the crystal packing as the crystal environment induced symmetry reduction (CEISR) effect. We believe that a new term is warranted because the observed phenomenon is not limited to this one case. Following the analysis of chloroazine **1**, we reviewed sixteen crystal structures of symmetrical azines that could be C_2 symmetric (Table 1). As with Table 3 for chloroazine **1**, we created intralayer and interlayer interaction inventories for crystals with similar supramolecular structures to **1** to examine the possible occurrence of CEISR. As can be seen, C_1 symmetry occurs for **2-Ia** (Br) and **10** (PrO), whereas C_2 symmetry occurs for **3** (I) and **5** (OPh). The results for **2-Ia** (Br) and **10** (PrO) are summarized on top of Table 5, those for **3** (I) and **5** (PhO) are

summarized on the bottom of Table 5, and the intermolecular pair interactions are described in Fig. S3–S6 (ESI†).

The entries in Table 5 show that the intramolecular contacts of **2-Ia** are qualitatively the same as those of **1-I**. The dominant intermolecular contacts again are Br···π interactions between bromoarenes. The f|Br(A_s) contact involves the bromine Br(A_s^*) and the face of the A_s arene in neighbor **X**, the Br|f(A_s) contact in Table 5. While the Cl···π contacts in **I** occur between pairs of chloroarenes, the Br···π contacts in **2-Ia** create chains (Fig. S10b, ESI†).

The arene inventory of **10** shows that the inside arene A_i^* engages in two T-contacts as a face (f|e_o(A_s) with **Q** and **U**) and in one more T-contact as an edge (e_o|f(A_s) with **T**). The surface arene A_s^* also engages in three T-contacts overall, but A_s^* serves as an edge twice (e_o|f(A_i) with **Q** and **U**) and as a face only once (f|e_o(A_i) with **T**). This difference between the coordination of A_i and A_s in the three arene–arene T-contacts already suffices to establish the inequivalence of A_i and A_s. Further evidence for their inequivalence is provided by the nature of the **R** contacts. The edge-H_{ortho} (e_o) of A_i^* engages in a contact with azine-N (e_o|Az and Az|e_o(A_i) with **R**) whereas A_s^* serves as a face in a contact with a methylene-H of the propoxyl group attached to A_i (f|CH_2(A_i) and CH_2|f(A_s) with **R**). While the edge of A_i^* engaged with neighbor **R** only uses its H_o, the other edge of A_i engaged with neighbor **T** employs both its H_o and H_m; H_o for the arene–arene T-contact and H_m for the contact with the propoxyl-O attached to A_s (e_m|O(A_s) with **T**).

The IAM architectures of **3** (I) and **5** (PhO) are easier to describe. These crystals contain C_2 symmetric azines and each azine engages its A_i and A_s arenes in four double T-contacts, two closed ones and two open ones (Table 5). Phenoxyazine **5** is special in that it exemplifies the first pair of azines featuring well defined quadruple T-contacts, and Fig. 7 exemplifies one such quadruple T-contact in pair **Q**. Not only do the A_i and A_s arenes engage in double T-contacts but the arenes of the phenoxy groups PhO_i and PhO_s also engage in T-contacts. Two more rows are needed in Table 5 to describe the arene–arene interactions between the phenoxy–phenyls and each T-contact is represented by one purple shaded cell.

The interlayer interactions involve only iodine–iodine bonding for **3** while the interlayer interactions for **5** are provided by face-to-face contacts between phenoxy–phenyls. We have pointed out the Az|e contacts as a prominent feature of the crystals with C_1-symmetric azines in **1-I**, **2-Ia** and **10** and these contacts only engage one arene (A_i) of the starred azine. In the crystals of the C_2-symmetric azines **3** and **5**, the Az|e contacts involve both A_i and A_s.

With this discussion of the structures of **2-Ia** (Br) and **10** (PrO), we have shown that their interaction inventories reflect the inequivalence of their two arenes just like we demonstrated for **1-I** (Cl) in Table 3. All three crystals with their C_1-symmetric azines have one shared feature that the option of four double T-contacts for intralayer interactions was forfeited to realize only three double T-contacts. This major inequivalence in A_i and A_s is reflected in all cases in a symmetry reduction from C_2-symmetry to C_1-symmetry. However, this symmetry reduction manifests itself in a more or less noticeable fashion. It just so happens that we first analyzed the azine with the smallest symmetry reduction. For **1**, the difference in the phenyl twists ϕ_1 = −29.31° and ϕ_2 = −30.53° is hardly noticeable, and this very small difference obfuscates the very significant difference in the coordination environments of its two arenes. The difference in the phenyl twists of **2-Ia** is more pronounced, ϕ_1 = −20.96° and ϕ_2 = −27.26°, and in **10** (PrO) the difference between ϕ_1 = −6.85° and ϕ_2 = −15.11° is even larger, and both cases provide clear manifestations of CEISR not only in the arene inventories but also in their molecular structures.

In the crystal structures that contain C_2-symmetric azines, the environments of arenes A_i and A_s are identical and the environments between *P*- and *M*-azines are enantiomeric, and therefore the electronic structures of A_i and A_s are the same. On the other hand, azines in crystal structures that feature CEISR contain arenes A_i and A_s as well as arene substituents X_i and X_s with different electronic structures, and these differences should manifest themselves in all kinds of measurements using vibrational (IR, Raman) or electron spectroscopy (UV/Vis, PES, XPS) as well as solid-state NMR spectroscopy.

2.5. Hirshfeld surface analyses

We have computed the Hirshfeld surfaces and the 2D Hirshfeld fingerprint plots for the (X,X)-azines using CrystalExplorer.[68–70] The results for chloroazine **1** and for all other azines are shown in Fig. S7 (ESI†).

The Hirshfeld fingerprint plots for **1-I** in Fig. S7 (ESI†) show information about the relative significance of the intralayer and interlayer contacts. The most crucial intralayer contacts are double T-contacts which constitute 28.2% of the full fingerprint plot. The spikes concentrated in the small light-blue regions in the C···H fingerprint plot correspond to C···H distances in double T-contacts. This feature supports the strong contribution of double T-contacts to intralayer binding, *i.e.*, the interactions between the starred molecule and the neighbors **Q**, **T** and **U**. The second type of purely intralayer contact, N···H contacts, constitutes 5.6% of the 2D fingerprint plot. The spikes in the fingerprint plot of N···H contacts are not very sharp which reflects their strengths. These correspond to the interaction between the starred molecule and the neighbors **V** and **W**.

The second type of intralayer contact, H···H contacts, is associated with more than 33.8% of the surface area of the fingerprint plot but has no spikes. The absence of spikes shows that these interactions are weaker. The fingerprint plot for these contacts includes the points corresponding to interlayer π···π contacts which we will discuss with the interlayer contacts. Lastly, the H···Cl contact which includes both the intralayer and interlayer contacts constitutes 25.9% of the area of the fingerprint plot. The spikes in the fingerprint plot reflect their significant contribution to the

Table 5 Intralayer and interlayer interaction inventories of flat symmetrical (X,X)-azines **2-Ia** (X = Br) and **10** (X = PrO) show crystal environment induced symmetry reduction (CEISR) whereas **3** (X = I) and **5** (X = PhO) show equivalent arenes

X	*(*P*)	Neighbors of the starred molecule[a]							
Br		**Q**(*M*)	**T**(*M*)	**R**(*M*)	**U**(*M*)	**V**(*P*)	**W**(*P*)		
Intra	A_i^*	f|e(A_s)	e|f(A_i)	Br|Me(A_s)	f|e(A_s)	vdW[b]	e|Az		
IAM	A_s^*	e|f(A_i)	f|e(A_s)	Me|Br(A_i)	e|f(A_i)	vdW[b]	vdW[b]		
	Az*				Az|Me(A_i)	Az|e(A_i)			
					Me(A_i)|Az				
		$\mathbf{Z}_1'(M)$	$\mathbf{Z}_1(M)$	**X**(*M*)	**X**(*M*)	$\mathbf{Z}_2(P)$	$\mathbf{Z}_2(P)$	**Y′**(*P*)	**Y**(*P*)
Inter	A_i^*	Br|e(A_s)						Br|Br(A_s)	
IAM	A_s^*		e|Br(A_i)	f|Br(A_s)	Br|f(A_s)	e|Br(A_s)	Br|e(A_s)		Br|Br(A_i)
PrO		**Q**(*M*)	**T**(*M*)	**R**(*M*)	**U**(*M*)				
Intra	A_i^*	f|e_o(A_s)	e_o|f(A_s)	e_o|Az	f|e_o(A_s)				
IAM	A_s^*	e_o|f(A_i)	f|e_o(A_i)	f|CH_2(A_i)	e_o|f(A_i)				
	A_i^*	O|e_m(A_s)	e_m|O(A_s)						
	A_s^*	e_m|O(A_i)	O|e_m(A_i)	CH_2|f(A_s)					
	Az*	Az|Me(A_s)	Az|Me(A_i)	Az|e_o(A_i)					
		Me(A_s)|Az	Me(A_i)|Az						
		Y(*P*)	**Y′**(*P*)	$\mathbf{Z}_1(P)$	$\mathbf{Z}_2(M)$	$\mathbf{Z}_3(M)$	$\mathbf{Z}_4(P)$		
Inter	A_i^*		Pr|O(A_s)			vdW[b]	vdW[b]		
IAM	A_s^*	O|Pr(A_i)		Pr|Pr(A_i)	vdW[b]				
I		**Q**(*M*)	**T**(*M*)	**R**(*M*)	**U**(*M*)				
Intra	A_i^*	f|e(A_s)	e|f(A_s)	e|f(A_s)	f|e(A_s)				
IAM	A_s^*	e|f(A_i)	f|e(A_i)	f|e(A_i)	e|f(A_i)				
	Az*	Az|Me(A_s)	Az|Me(A_i)	Az|e(A_i)	Az|e(A_s)				
		Me(A_s)|Az	Me(A_i)|Az	e(A_i)|Az	e(A_s)|Az				
				X(*P*)	**X′**(*P*)				
Inter	A_i^*				I|I(A_s)				
IAM	A_s^*			I|I(A_i)					
PhO		**Q**(*M*)	**T**(*M*)	**R**(*M*)	**U**(*M*)				
Intra	A_i^*	f|e(A_s)	e|f(A_s)	e|f(A_s)	f|e(A_s)				
IAM	A_s^*	e|f(A_i)	f|e(A_i)	f|e(A_i)	e|f(A_i)				
	PhO_i^*	e|f(PhO_s)	f|e(PhO_s)	f|e(PhO_s)	e|f(PhO_s)				
	PhO_s^*	f|e(PhO_i)	e|f(PhO_i)	e|f(PhO_i)	f|e(PhO_i)				
	Az*	Az|Me(A_s)	Az|Me(A_i)	Az|e(A_i)	Az|e(A_s)				
		Me(A_s)|Az	Me(A_i)|Az	e(A_i)|Az	e(A_s)|Az				
		X(*M*) & **Y**(*M*)		**X′**(*M*) & **Y′**(*M*)		**Z and Z′**			
Inter	A_i^*	PhO|PhO(A_s)				vdW[b]			
IAM	A_s^*			PhO|PhO(A_i)		vdW[b]			

[a] See Fig. S3–S6 (ESI†) for definition of intralayer and interlayer neighbors. [b] vdW = non-specific van der Waals interaction.

intralayer binding. The interaction between the starred molecule and the neighbor **R** corresponds to this contact.

Next, we discuss the contributions to the interlayer binding, which comes from three types of contacts, H···Cl, Cl···Cl and π···π contacts. The first and most important interlayer contacts, H···Cl contacts, appear as sharp spikes in the fingerprint plot which reflect their significant contribution to the interlayer binding. This corresponds to the interactions between the starred molecule and the neighbors $\mathbf{Z}_1$, $\mathbf{Z}_1'$, and $\mathbf{Z}_2$. The second type of contact, Cl···Cl contacts, constitutes only 2.1% of the area of the fingerprint plot. The spike in the plot indicates a directional interlayer binding interaction. This corresponds to the interaction between the starred molecule and the neighbors **Y** and **Y′**. The last and another important contact is the π···π contact which appears in the mid region of the H···H plots and also contributes to the interlayer binding. These close contacts result from the

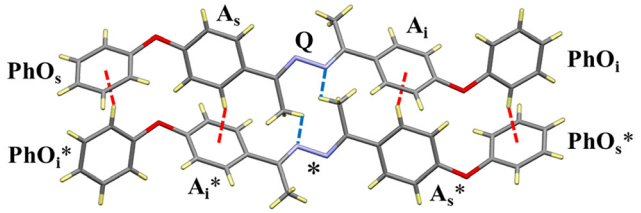

Fig. 7 The pair **Q** of phenoxyazine **5** illustrates an arene–arene quadruple T-contact. See text for details.

Cl···π interaction between the starred molecule and the neighbor **X**.

The inspection of Hirshfeld 2D fingerprint plots resolved into N···H contacts allows one to decide whether an acetophenone azine crystallizes with or without CEISR. This information is easily accessible and does not rely on structural analysis. Fig. 9 shows the respective plots for the five azines analyzed. The pattern displayed by the crystals with C_2-symmetric azines resembles a flower with four petals, two sets that are symmetric about the diagonal. One set with the shorter N···H contacts is due to Az|Me contacts (dark-blue in Fig. 8) and the other set with the longer N···H contacts is due to Az|e contacts (light-red in Fig. 8). The pattern becomes complex for the crystals with C_1-symmetric azines. The longitudinal offset between pairs of azines in the crystal structures leads to a curtain like pattern instead of the two distinct sets of petals.

2.6. Pairwise interaction energies and electrostatic potential maps

Our crystal structure analyses revealed short contacts between synthons and their directionality, and we will now quantify the interactions. Pairwise interaction energies were computed with CrystalExplorer at the CE-B3LYP level, that is, B3LYP/6-31G(d,p)+D2 for all intra- and interlayer pairs within 3.8 Å of the selected reference molecule * in chloroazine **1-I**, bromoazine **2-Ia**, and propoxyazine **10**. We also analyzed phenoxyazine **5** and iodoazine **3** to establish a reference for a case with intralayer interactions greatly dominating over interlayer interactions. The calculations result in color-coded interaction energy mappings and the results for the chloroazine and the other azines are given in Fig. S8–S12 (ESI†). In Table 6 are listed the most pertinent pair interaction energies between the starred molecule and neighbor specified in column 1. In Table S2 (ESI†), also are provided for each pair, the electrostatic (E_{ele}), polarization (E_{pol}), dispersion (E_{dis}), and exchange-repulsion (E_{xrep}) terms together with the sum of all energy components (E_{tot}).

To obtain a first impression of the relative strengths of the pair interactions, we categorized the total energies as follows: weak (0–4 kJ mol^{-1}, black), moderate (4–15 kJ mol^{-1}, red), strong (15–50 kJ mol^{-1}, **bold red**), and superior (above 50 kJ mol^{-1}, burgundy).

The **U** pair in chloroazine **1-I** features a double T-contact with the least longitudinal offset and the associated pair energy shows significantly stronger bonding compared to the double T-contacts in pairs **Q**, **T**, and **R**. Note the inverse correlation between the E_{tot} and R values, which specify the distance between the molecular centroids and provide a rough measure of the longitudinal offset. Considering the data for the **U** pair suggests a binding energy for a strong T-contact between two *para*-disubstituted arenes (*i.e.*, *p*-substituted 1-iminomethylbenzenes) of about E_b(T,ds) = −23 kJ mol^{-1}. The longitudinal offsets of the quadruple T-contacts in phenoxyazine **5** are very close to that of pair **U** in **1-I** and hence one might expect a binding energy of −92 kJ mol^{-1}. The actual binding energies of pairs **Q**, **T**, **R**, and **U** in **5** are close to −70 kJ mol^{-1}, and these numbers suggest that the

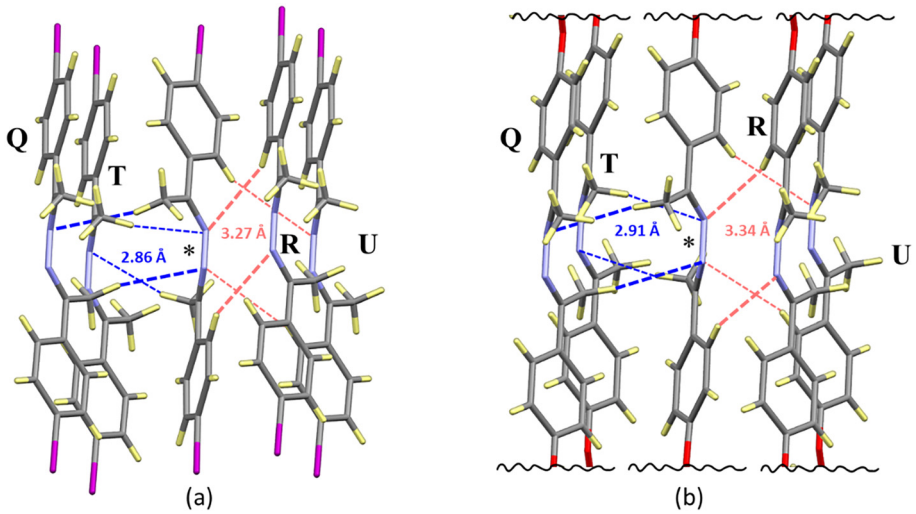

Fig. 8 The starred molecule in the center of (a) **3** (I) and (b) **5** (PhO)–azines engages its azine moiety with both of its arenes A$_i$ and A$_s$ in e|Az and Az|e contacts, shown in light red (**R** and **U**), and it also engages its azine moiety in Me|Az and Az|Me contacts with the methyl groups, shown in dark blue (**Q** and **T**).

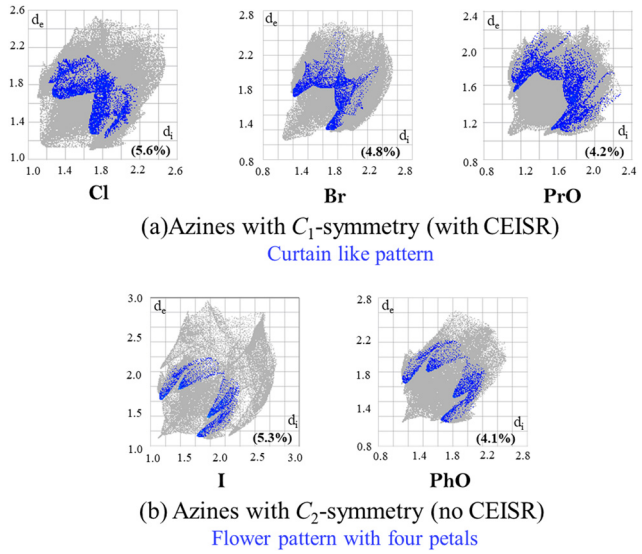

Fig. 9 Hirshfeld 2D fingerprint plots for (X,X)-azines resolved into N···H contacts for azines (a) with C_1-symmetry and (b) with C_2-symmetry.

T-contacts between the phenoxy groups are less bound than the T-contacts involving arenes A_i and A_s. Assuming to a first approximation that the T-contacts involving A_i and A_s are about the same, one would conclude that the terminal T-contacts involving two mono-substituted arenes (*i.e.*, phenoxy groups) contribute only about E_b(T,ms) = −12 kJ mol^{-1} to the pair binding energy. Of course, the E_b(T,ds) and E_b(T,ms) terms are not transferable from one azine to the next because the details of the T-contact structures vary (distance, offset). However, it is safe to say that E_b(T,ms) < E_b(T,ds) and electrostatic potential maps provide a clear rationale.

The electrostatic potential maps of azines **1**, **2**, and **5** are shown in Fig. 10 along with the maps of the respective benzenes Ph–X. The B3LYP/6-311G(d,p) electron densities were computed based on the partially optimized structures of the azines (X-ray structure with H positions optimized) and the fully optimized Ph–X structures. Two perspectives are shown for each azine with their C_2-axis perpendicular to the paper plane and viewing the convex (top) and concave surfaces. To the right are shown the map of the azine viewed down the N–N axis and the map of the respective Ph–X.

All X_{para} groups are −I/+M substituents.[71] The ESP maps of the Ph–X molecules feature positive potential at all aromatic hydrogens reflecting the −I property of X. The halogens show their usual red ring of negative potential and a more or less developed σ-hole. Note the negative potential on the face of the phenyl ring which is consistent with the +M effect. The magnitude of the +M effect greatly depends on the overlap between the π-densities of the X group and the arene. The orbital expansions of the arene carbons match much better for the OR substituent than for the larger halogens, and the strong +M effect is clearly visible in Fig. 10.

The azine group is a −I/−M substituent. The first consequence of the overall electron withdrawing ability of the azine group is an area of intense negative potential associated with the N_2 group visible only on the convex face of the azine. Because of the azine twist angle, the convex and concave faces are remarkably different. The dominant feature on the concave face of the azine are the two areas of positive potential and each of these includes two edge Hs and two of the methyl Hs. Note the marked difference in the electrostatic potential of the methyl H pointed towards the lone pair of one of the azine Ns. It is a common feature of the azines that the edge regions of both arenes on the convex face of the azine indicate much lower electrophilicity for just the two Hs as compared to the expansive region of high electrophilicity associated with four Hs on the concave face.

The combination of the azine −I/−M effect with the −I/+M *para*-substituent has several consequences. The two

Table 6 Color-coded pairwise interaction energies relative to the starred molecule in **5** (PhO), **3** (I), **1-I** (Cl), **2-Ia** (Br) and **10** (PrO)

With CEISR					
Cl	E_{tot}[a]	**Br**	E_{tot}[a]	**PrO**	E_{tot}[a]
U	**−45.6**	**U**	**−43.5**	**U**	**−68.1**
Q, T	**−34.4**	**Q, T**	**−37.7**	**T**	**−67.2**
V, W	**−33.7**	**V, W**	**−30.3**	**Q**	**−65.4**
R	−11.8	**X**	**−30.3**	**R**	**−62.3**
Z_1	−7.5	**R**	**−19.0**	**S**	**−37.0**
Z_2	−4.2	**Z_1**	−7.4	**Y**	−11.9
X	−3.0	**Y**	−5.5	**Z_1**	−9.9
Y	0.2	**Z_2**	−3.9	**Z_2**	−6.2
				Z_3	−3.7
				Z_4	−2.3

Without CEISR			
PhO	E_{tot}[a]	**I**	E_{tot}[b]
Q, T	**−70.6**	**R, U**	**−52.9**
R, U	**−67.9**	**Q, T**	−49.2
S	−26.0	**S**	−27.5
Y	−7.9	**Y**	6.2
X	−6.0		
Z	−4.4		

[a] E_{tot} (CE-B3LYP) = 1.057 E_{ele} + 0.740 E_{pol} + 0.871 E_{dis} + 0.618 E_{xrep} for **5** (PhO), **1-I** (Cl), **2-Ia** (Br) and **10** (PrO). [b] E_{tot} (CE-HF) = 1.019 E_{ele} + 0.651 E_{pol} + 0.901 E_{dis} + 0.811 E_{xrep} for **3** (I).

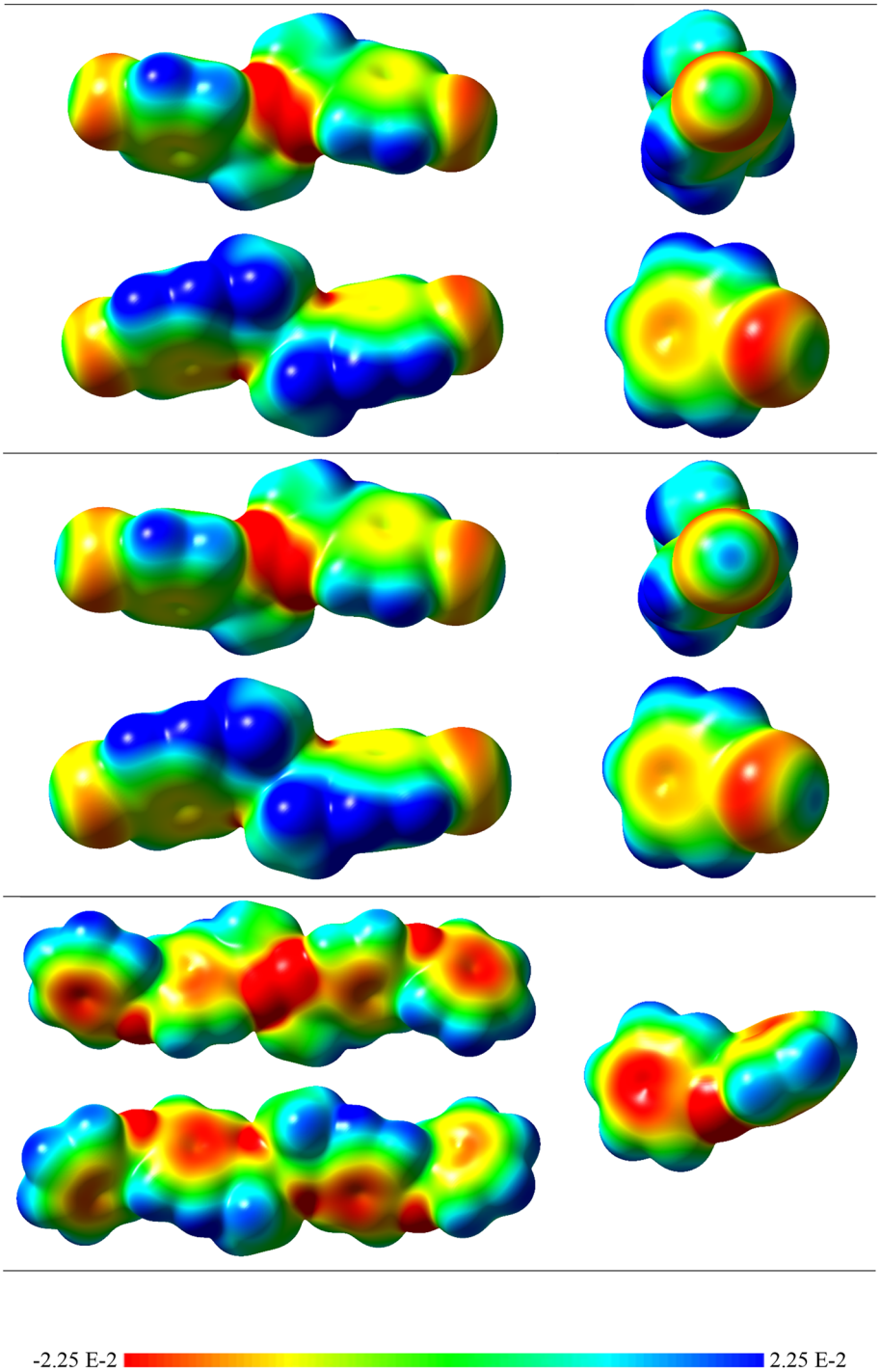

Fig. 10 Electrostatic potential (ESP) maps of the symmetrical (X,X) acetophenone azines and of the monosubstituted benzenes Ph–X with X = Cl (top), Br (middle), and PhO (bottom). ESPs are mapped on electron density isosurfaces with ρ = 0.001 e au^{-3} and the ESP values are color-coded as shown. See text for orientations.

overall electron withdrawing substituents in (X,X)-azines compete for electron density from four arene Hs whereas the one substituent in a Ph–X molecule may draw electron density from five arene Hs. This fact in combination with the discussed difference between the edges on the convex and concave faces makes it clear that the edge electrophilicity on the convex face is greatly diminished compared to Ph–X while the edge electrophilicity on the convex face exceeds that of Ph–X by a greater amount. The combination of the azine −M effect with the +M effect of the X group results in reduced nucleophilicity on both arene faces, and the reduction of nucleophilicity is more pronounced on the convex face (green–yellow) than on the concave face (red–yellow).

3. Conclusion

Ab initio studies show that the molecular structure of (*E*,*E*)-configured *p*-chloroacetophenone azine **1** is C_2-symmetric in the gas phase. Furthermore, computational analysis shows that the azine twist angle and the phenyl twists are correlated in a manner that minimizes the intersection angle between the best planes of the two arenes in one azine molecule. The crystal structure of polymorph **1-I** contains equal amounts of enantiomers which are very nearly but not exactly C_2-symmetric: the molecules are asymmetric rather than dissymmetric. We have provided several lines of evidence to show that the modest $C_2 \rightarrow C_1$ symmetry reduction of the azines in the crystal is due to the crystal architecture: the inside arene A_i and the surface arene A_s in each azine engage in qualitatively different intermolecular interactions. We refer to this consequence of the crystal packing as the crystal environment induced symmetry reduction (CEISR) effect. A new term is warranted because the observed phenomenon is not limited to this one case (Table 1).

The analysis of the crystal architecture emphasizes the importance of arene–arene and chloroarene–chloroarene interactions and resulted in the intralayer and interlayer interaction inventory presented in Table 3 and the structural characteristics of each synthon in Table 4. The deep analyses revealed a remarkable and non-obvious qualitative difference between the coordination modes of arenes A_i and A_s in the intralayer namely that only A_i engages in arene–azine contacts. While it was this analysis of the arene–azine contacts that initially brought this inequivalence to our attention, the analysis of the arene–arene contacts is comparatively easier to perform for the demonstration of the inequivalence. While azines have the potential to form four double T-contacts, the arenes A_i and A_s in **1-I** engage only in three double T-contacts. The arene A_i serves as a face twice and only once as an edge while the arene A_s serves as an edge twice and only once as a face. The unexploited edge of A_i engages in the intralayer arene–azine contact while the remaining face of the A_s participates in interlayer contacts.

The inequivalence of arenes in the intralayer has a direct consequence on the contacts of both the arenes in the interlayer. Two main types of interlayer contacts, the f|Cl type between a chlorine of one chloroarene and an arene face of the other chloroarene, and the Cl|e type between a chlorine of one chloroarene and a hydrogen of the other chloroarene (the edge-H *meta* to the azine), occur. Only the arene A_s engages in two f|Cl type contacts as listed in Table 3 and no such contact occurs for the inside arene A_i. The arene A_s is clearly much more engaged in the interlayer contacts compared to the A_i arene which is also true for the Cl|e type contacts. A_s engages in three Cl|e contacts while A_i engages in only one such contact (Fig. 6).

To explore the generality of the CEISR concept, we studied the IAM characteristics of the four other azines that crystallize with a flat morphology **2-Ia** (Br), **3** (I), **5** (PhO), and **10** (PrO). The interaction inventories in Table 5 show that the two arenes in azines **2-Ia** and **10** engage in three inequivalent double T-contacts as in **1-I**. Only the inside arene is engaged in the arene–azine contact. The interlayer contacts are also different for both the arenes because of the differences in the contacts within the intralayer. On the other hand, the crystal structures of **3** and **5** feature two equivalent coordination modes for both arenes.

Comprehensive interaction inventory analysis is a powerful method to detect CEISR. However, this topological analysis is an arduous task, and it is easily possible to overlook significant contacts only revealed by pairwise interaction energy analyses. We showed that N···H contact Hirshfeld 2D fingerprint plot analyses provide the fastest and most direct method for the detection of CEISR. The plots in Fig. 10 show similar curtain like patterns for crystals **1-I**, **2-Ia**, and **10** in evidence of CEISR while the plots for **3** and **5** show a flower pattern with two distinct set of petals indicative of arene equivalence.

Azines in crystal structures that feature CEISR contain arenes A_i and A_s as well as arene substituents X_i and X_s with different electronic structures. These differences should manifest themselves in measurements using vibrational spectroscopy (IR, Raman) and electron spectroscopy (UV/Vis, PES, XPS), as well as solid-state NMR spectroscopy. The availability of the series of (X,X)-disubstituted acetophenone azines allows for such systematic studies going forward.

The results of our studies suggest that the crystallographic record contains many crystal structures for which packing related molecular symmetry reductions may not have been fully recognized. In our approach, we compared the next neighbor interactions of two arenes and showed them to be different. The approach does not rely on the presence of arenes and can be generalized to any molecular system with two moieties of the same constitution.

Author contributions

H. Bhoday and K. Yang: synthesis and crystallization, formal analysis, computational analysis, methodology, visualization, writing; S. P. Kelley: X-ray crystallography, X-ray data curation; R. Glaser: conceptualization, formal analysis, methodology, visualization, funding acquisition, project administration, resources, supervision and mentoring, writing.

Conflicts of interest

The authors declare no conflicts of interest.

Acknowledgements

This work was supported by the Missouri University of Science and Technology and, in part, by a grant from the National Science Foundation #1665487.

References

1 S. S. Chourasiya, D. Kathuria, A. A. Wani and P. V. Bharatam, Azines: Synthesis, Structure, Electronic Structure and Their Applications, *Org. Biomol. Chem.*, 2019, **17**, 8486–8521.

2 J. Galeta, S. Man, A. Valoušková and M. Potáček, Substituted homoallenyl and their derivatives. Part 2: Azines, *Chem. Pap.*, 2013, **67**, 40–50.
3 M. J. Naim, O. Alam, M. F. Nawaz, J. Alam and P. Alam, Current status of pyrazole and its biological activities, *J. Pharm. BioAllied Sci.*, 2016, **8**, 2–17.
4 L. Subedi, O. W. Kwon, C. Pak, G. Lee, K. Lee, H. Kim and S. Y. Kim, N,N-disubstituted azines attenuate LPS-mediated neuroinflammation in microglia and neuronal apoptosis via inhibiting MAPK signaling pathways, *BMC Neurosci.*, 2017, **18**, 1–12.
5 V. B. Kurteva, S. P. Simeonov and M. Stoilova-Disheva, Symmetrical Acyclic Aryl Aldazines with Antibacterial and Antifungal Activity, *Pharmacol. Pharm.*, 2011, **2**, 1–9.
6 C. Liang, J. Xia, D. Lei, X. Li, Q. Yao and J. Gao, Synthesis, in vitro and in vivo antitumor activity of symmetrical bis-Schiff base derivatives of isatin, *Eur. J. Med. Chem.*, 2014, **74**, 742–750.
7 A. Paterna, R. Khonkarn, S. Mulhovo, A. Moreno, P. M. Girio, H. Baubichon-Cortay, P. Falson and M. J. U. Ferreira, Monoterpene indole alkaloid azine derivatives as MDR reversal agents, *Bioorg. Med. Chem.*, 2018, **26**, 421–434.
8 J. A. Jedryka, K. Bijak, D. Sek, M. Siwy, M. Filapek, G. Malecki, S. Kula, G. Lewinska, M. E. Nowak, J. Sanetra, H. Janeczek, K. Smolarek, S. Mackowski and S. E. Balcerzak, Unsymmetrical and symmetrical azines toward application in organic photovoltaic, *Opt. Mater.*, 2015, **39**, 58–68.
9 V. S. Vyas, F. Haase, L. Stegbauer, G. Savasci, F. Podjaski, C. Ochsenfeld, V. Bettina and V. Lotsch, A tunable azine covalent organic framework platform for visible light-induced hydrogen generation, *Nat. Commun.*, 2015, **6**, 1–9.
10 P. Acker, M. E. Speer, J. S. Wössner and B. Esser, Azine-based polymers with a two-electron redox process as cathode materials for organic batteries, *J. Mater. Chem. A*, 2020, **8**, 11195–11201.
11 B. Vercelli, M. Pasini, A. Berlin, J. Casado, J. T. L. Navarrete, R. P. Ortiz and G. Zotti, Phenyl- and Thienyl-Ended Symmetric Azomethines and Azines as Model Compounds for n-Channel Organic Field-Effect Transistors: An Electrochemical and Computational Study, *J. Phys. Chem. C*, 2014, **118**, 3984–3993.
12 W. Hong, C. Guo, B. Sun and Y. Li, (3Z,3′Z)-3,3′-(Hydrazine-1,2-diylidene)bis(indolin-2-one) as a new electron-acceptor building block for donor–acceptor π-conjugated polymers for organic thin film transistors, *J. Mater. Chem. C*, 2015, **3**, 4464–4470.
13 M. Lewis, C. L. Barnes and R. Glaser, 4-Chloroacetophenone-(4-methoxyphenylethylidene) hydrazone, *Acta Crystallogr., Sect. C: Cryst. Struct. Commun.*, 2000, **56**, 393–396; M. Lewis, C. L. Barnes and R. Glaser, CSD Communication, 2000, CCDC 143276 (CODRES).
14 G. S. Chen, J. K. Wilbur, C. L. Barnes and R. Glaser, Push-Pull Substitution versus Intrinsic or Packing Related N-N Gauche Preferences in Azines. Synthesis, Crystal Structures and Packing of Asymmetrical Acetophenone Azines, *J. Chem. Soc., Perkin Trans. 2*, 1995, 2311–2317; G. S. Chen, J. K. Wilbur, C. L. Barnes and R. Glaser, CSD Communication, 1996, CCDC 1312232 (ZIFBUL).
15 M. Lewis, C. L. Barnes and R. Glaser, Near-Perfect Dipole Parallel-Alignment in the Highly Anisotropic Crystal Structure of 4-Iodoacetophenone-(4-methoxyphenylethylidene) Hydrazone, *J. Chem. Crystallogr.*, 2000, **30**, 489–496; M. Lewis, C. L. Barnes and R. Glaser, CSD Communication, 2001, 165429 (SUXZAM).
16 M. Lewis, H. Bhoday, C. L. Barnes, S. P. Kelley and R. Glaser, Para-Chloroacetophenone para-Phenoxyacetophenone Azine (100 K), CSD Communication, 2020, CCDC 2017223 (NUVPUS).
17 M. Lewis, H. Bhoday, A. Choudhury, S. P. Kelley, C. L. Barnes and R. Glaser, Para-Bromoacetophenone para-Phenoxyacetophenone Azine (100 K), CSD Communication, 2020, CCDC 2014691 (KUSNEU).
18 M. Lewis, H. Bhoday, C. L. Barnes, S. P. Kelley, A. Choudhury and R. Glaser, Para-Iodoacetophenone para-Phenoxyacetophenone Azine (173 K), CSD Communication, 2020, CCDC 2017222 (NUVPOM).
19 H. Bhoday, S. P. Kelley and R. Glaser, CSD Communication, 2021, CCDC 2103130 (XUXDIG02, a.k.a. OBELIU).
20 H. Bhoday, M. Lewis, S. P. Kelley and R. Glaser, Perfect Polar Alignment of Parallel Beloamphiphile Monolayers: Synthesis, Characterization, and Crystal Architectures of Unsymmetrical Phenoxy-Substituted Acetophenone Azines, *ChemPlusChem*, 2022, **87**, e202200224, 1–7.
21 H. Bhoday, S. P. Kelley and R. Glaser, Polar and non-polar stacking of perfectly aligned parallel beloamphiphile monolayers (PBAMs) of (PhO, F)-azine. The interplay of non-covalent interlayer interactions and unit cell polarity, *CrystEngComm*, 2023, **25**, 2175–2180.
22 R. Glaser, N. Knotts, P. Yu, L. Li, M. Chandrasekhar, C. Martin and C. L. Barnes, Perfect polar stacking of parallel beloamphiphile layers, Synthesis, structure, and solid-state optical properties of the unsymmetrical acetophenone azine DCA, *Dalton Trans.*, 2006, 2891–2899.
23 N. Knotts, R. Glaser, C. Barnes and S. P. Kelley, 4-Decyloxyacetophenone 4-Fluoroacetophenone Azine, CSD Communication, 2020, CCDC 2040896 (XUYYEY).
24 N. Knotts, R. Glaser, C. Barnes and S. P. Kelley, 4-Decyloxyacetophenone 4-Chloroacetophenone Azine. CSD Communication, 2020, CCDC 2040898 (XUYYOI).
25 N. Knotts, R. Glaser, C. Barnes and S. P. Kelley, 4-Decyloxyacetophenone 4-Bromoacetophenone Azine. CSD Communication, 2020, CCDC 2040895 (XUYYAU).
26 R. Glaser, Polar Order by Rational Design: Crystal Engineering With Parallel Beloamphiphile Monolayers, *Acc. Chem. Res.*, 2007, **40**, 9–17.
27 M. Lewis, Z. Wu and R. Glaser, *Arene-Arene Double T-Contacts. Lateral Synthons in the Engineering of Highly Anisotropic Organic Crystals in Anisotropic Organic Materials – Approaches to Polar Order*, ed. R. Glaser and P. Kaszynski, ACS Symposium Series, American Chemical Society, Washington, D.C., 2001, ch. 7, vol. 798, pp. 97–111.

28 M. Lewis and R. Glaser, The Azine Bridge as a Conjugation Stopper: An NMR Spectroscopic Study of Electron Delocalization in Acetophenone Azines, *J. Org. Chem.*, 2002, **67**, 1441–1447.
29 R. Glaser, G. S. Chen and C. L. Barnes, Conjugation in azines. Stereochemical analysis of benzoylformate azines in the solid state, in solution, and in the gas phase, *J. Org. Chem.*, 1994, **58**, 7446–7455.
30 R. Glaser, G. S. Chen, M. Anthamatten and C. L. Barnes, Stereochemistry and Stereoelectronics of Azines. A Solid-State Study of Symmetrical, (E,E)-Configured, Para-Substituted (H, F, Cl, Br, CN) Acetophenone Azines, *J. Org. Chem.*, 1994, **59**, 4336–4340.
31 J. Grzegorzek, Z. Mielke and A. Filarowski, C=N-N=C conformational isomers of 2′-hydroxyacetophenone azine: FTIR matrix isolation and DFT study, *J. Mol. Struct.*, 2010, **976**, 371–376.
32 R. Glaser, G. S. Chen, M. Anthamatten and C. L. Barnes, Polymorphism and Conformational C=N-N=C Bond Isomers of Azines: X-Ray Crystal and ab Initio Structures of Two Rotameric Structures of Methyl (para-Tolyl) Ketone Azine, *Angew. Chem., Int. Ed. Engl.*, 1994, **33**, 1081–1083.
33 M. Lewis, C. L. Barnes and R. Glaser, The Crystal Structure of 4-Iodoacetophenone Azine, *J. Chem. Crystallogr.*, 1999, **29**, 1043–1048.
34 S. Tighdouini, S. Radi, L. Toupet, M. Sirajuddin, T. B. Hadda, M. Akkurt, I. Warad, Y. N. Mabkhot and S. Ali, *J. Chem. Sci.*, 2015, **127**, 2211–2216.
35 S. P. Kelley, C. L. Barnes, J. Ratchford, K. Yang, N. Corretjer and R. E. Glaser, CSD Communication, 2018, CCDC 1843926 (WEWMET).
36 H. Bhoday, A. Schuman, K. Yang, S. P. Kelley and R. Glaser, CSD Communication, 2020, CCDC 2027208 (HUXMIZ).
37 M. Lewis, *PhD thesis*, University of Missouri, 2001.
38 H. Bhoday, A. Schuman, S. P. Kelley and R. Glaser, CSD Communication, 2020, CCDC 2027206 (HUXMEV).
39 G. S. Chen, M. Anthamatten, C. L. Barnes and R. Glaser, CSD Communication, 1995, CCDC 1207288 (LIKJEU).
40 M. Lewis, C. L. Barnes and R. Glaser, CSD Communication, 2000, CCDC 139916 (LIZNEN).
41 C. L. Barnes, S. P. Kelley, M. Lewis and R. Glaser, CSD Communication, 2018, CCDC 1838227 (KIGBAG).
42 H. Bhoday, A. Schuman, K. Yang, S. P. Kelley and R. Glaser, CSD Communication, 2020, CCDC 2027208 (HUXMIX).
43 G. P. Moss, Basic Terminology of Stereochemistry (IUPAC Recommendations 1996), *Pure Appl. Chem.*, 1996, **68**, 2193–2222.
44 H. A. Favre and W. H. Powell, *Nomenclature of Organic Chemistry: IUPAC Recommendations and Preferred Names*, Royal Society of Chemistry, UK, 2013.
45 R. G. Parr and W. Yang, *Density-Functional Theory of Atoms and Molecules*, Oxford University Press, New York, Oxford, 1989.
46 A. Austin, G. Petersson, M. J. Frisch, J. Dobek, G. Scalmani and K. Throssell, A Density Functional with Spherical Atom Dispersion Terms, *J. Chem. Theory Comput.*, 2012, **8**, 4989–5007.
47 A. D. Mclean and G. S. Chandler, Contracted Gaussian Basis Sets for Molecular Calculations 1. 2nd Row Atoms, Z = 11-18, *J. Chem. Phys.*, 1980, **72**, 5639–5648.
48 K. Raghavachari, J. S. Binkley, R. Seeger and J. A. Pople, Self-Consistent Molecular Orbital Methods. 20. Basis Set for Correlated Wave-Functions, *J. Chem. Phys.*, 1980, **72**, 650–654.
49 M. J. Frisch, A. People and J. S. Binkley, Self-Consistent Molecular Orbital Methods. 25. Supplementary Functions for Gaussian Basis Sets, *J. Chem. Phys.*, 1984, **80**, 3265–3269.
50 M. J. Frisch, G. W. Trucks, H. B. Schlegel, G. E. Scuseria, M. A. Robb, J. R. Cheeseman, G. Scalmani, V. Barone, G. A. Petersson, H. Nakatsuji, X. Li, M. Caricato, A. V. Marenich, J. Bloino, B. G. Janesko, R. Gomperts, B. Mennucci, H. P. Hratchian, J. V. Ortiz, A. F. Izmaylov, J. L. Sonnenberg, D. Williams-Young, F. Ding, F. Lipparini, F. Egidi, J. Goings, B. Peng, A. Petrone, T. Henderson, D. Ranasinghe, V. G. Zakrzewski, J. Gao, N. Rega, G. Zheng, W. Liang, M. Hada, M. Ehara, K. Toyota, R. Fukuda, J. Hasegawa, M. Ishida, T. Nakajima, Y. Honda, O. Kitao, H. Nakai, T. Vreven, K. Throssell, J. A. Montgomery Jr. , J. E. Peralta, F. Ogliaro, M. J. Bearpark, J. J. Heyd, E. N. Brothers, K. N. Kudin, V. N. Staroverov, T. A. Keith, R. Kobayashi, J. Normand, K. Raghavachari, A. P. Rendell, J. C. Burant, S. S. Iyengar, J. Tomasi, M. Cossi, J. M. Millam, M. Klene, C. Adamo, R. Cammi, J. W. Ochterski, R. L. Martin, K. Morokuma, O. Farkas, J. B. Foresman and D. J. Fox, *Gaussian 16, Revision C.01*, Gaussian, Inc., Wallingford CT, 2016.
51 R. Glaser, G. S. Chen, M. Anthamatten and C. L. Barnes, Comparative Analysis of Crystal Structures of (E,E)-Configured para-Substituted Acetophenone Azines with Halogen, Oxygen, Nitrogen, and Carbon Functional Groups, *J. Chem. Soc., Perkin Trans. 2*, 1995, 1449–1458.
52 H. Bhoday, S. P. Kelley and R. Glaser, CSD Communication, 2023, CCDC 2241667 (LEXTIV).
53 E. Arunan and H. S. Gutowsky, The rotational spectrum, structure and dynamics of a benzene dimer, *J. Chem. Phys.*, 1993, **98**, 4294–4296.
54 A. Katrusiak, M. Podsiadzo and A. Budzianowski, Association CH···π and No van der Waals Contacts at the Lowest Limits of Crystalline Benzene I and II Stability Regions, *Cryst. Growth Des.*, 2010, **10**, 3461–3465.
55 R. Glaser, M. Lewis and Z. Wu, Conformational Effects on The Quadrupolarity of Azines. An ab Initio Quantum-Mechanical Study of a Lateral Synthon, *J. Mol. Model.*, 2000, **6**, 86–98.
56 H. Matter, M. Nazar, S. Gssregen, D. W. Will, H. Schreuder, A. Bauer, M. Urmann, K. Ritter, M. Wagner and V. Wehner, Evidence for CCl/CBr···pi Interactions as an Important

Contribution to Protein–Ligand Binding Affinity, *Angew. Chem., Int. Ed.*, 2009, **48**, 2911.
57 Y. N. Imai, Y. Inoue, I. Nakanishi and K. Kitaura, Cl-π Interactions in Protein-Ligand Complexes, *Protein Sci.*, 2008, **17**, 1129–1137.
58 J. R. Ovens and D. B. Lenzoff, Probing halogen···halogen interactions via thermal expansion analysis, *CrystEngComm*, 2018, **20**, 1769.
59 M. C. Cortada, J. Castelló and J. J. Novoa, The nature of the C–Cl···Cl–C intermolecular interactions found in molecular crystals: a general theoretical-database study covering the 2.75–4.0 Å range, *CrystEngComm*, 2014, **16**, 8232.
60 N. K. Nath and P. Naumov, In Situ Crystallization and Crystal Structure Determination of Chlorobenzene, *Maced. J. Chem. Chem. Eng.*, 2015, **34**, 63.
61 P. K. Thallapally and A. Nangia, A Cambridge Structural Database analysis of the C–H···Cl interaction: C–H···Cl2 and C–H···Cl–M often behave as hydrogen bonds but C–H···Cl–C is generally a van der Waals interaction, *CrystEngComm*, 2001, **27**, 1–6.
62 D. Swierczynski, R. Luboradzki, G. Dolgonos, J. Lipkowski and H. J. Schneider, Non-Covalent Interactions of Organic Halogen Compounds with Aromatic Systems – Analyses of Crystal Structure Data, *Eur. J. Org. Chem.*, 2005, 1172–1177.
63 M. Nishio, The CH/π hydrogen bond in chemistry. Conformation, supramolecules, optical resolution and interactions involving carbohydrates, *Phys. Chem. Chem. Phys.*, 2011, **13**, 13873.
64 M. Lewis, C. Bagwilla, L. Hardebecka and S. Wireduaaha, Modern Computational Approaches to Understanding Interactions of Aromatics, in *Aromatic Interactions: Frontiers in Knowledge and Application*, Royal Society of Chemistry, 2017, ch. 1.
65 H. Li, Y. Lu, Y. Liu, X. Zhu, H. Liu and W. Zhu, Interplay between halogen bonds and π–π stacking interactions: CSD search and theoretical study, *Phys. Chem. Chem. Phys.*, 2012, **14**, 9948.
66 T. Dahl, The nature of stacking interactions between organic molecules elucidated by analysis of crystal structures, *Acta Chem. Scand.*, 1994, **48**, 95.
67 D. Britton and W. W. Brennessel, p-Chloro-, p-bromo- and two polymorphs of p-iodoacetophenone, *Acta Crystallogr., Sect. C: Cryst. Struct. Commun.*, 2004, **60**, o552.
68 M. A. Spackman, A. S. Mitchell and J. J. McKinnon, Hirshfeld Surfaces: A New Tool for Visualising and Exploring Molecular Crystals, *Chem. – Eur. J.*, 1998, **4**, 2136–2141.
69 M. A. Spackman and D. Jayatilaka, Hirshfeld surface analysis, *CrystEngComm*, 2009, **11**, 19–32.
70 J. J. McKinnon, M. A. Spackman and A. S. Mitchell, Novel tools for visualizing and exploring intermolecular interactions in molecular crystals, *Acta Crystallogr., Sect. B: Struct. Sci.*, 2004, **60**, 627–668.
71 C. Hansch, A. Leo, R. W. Taft and A. S. Mitchell, A survey of Hammett Substituent Constants and Resonance and Field Parameters, *Chem. Rev.*, 1991, **91**, 165–195.